Distribution and Genetic Structure of the Sierra Nevada red fox in Oregon

GPS-collared Sierra Nevada red fox female, OR-SNRF-01, from central Oregon Cascades. Photo Credit: Tim L. Hiller

Final Report
Prepared for the Oregon Department of Fish and Wildlife
Salem, OR
Agreement No. 379-15

Prepared by:

Cate B. Quinn[a], Tim L. Hiller[b], Benjamin N. Sacks[a]

[a] *Mammalian Ecology and Conservation Unit, Veterinary Genetics Laboratory; Department of Population Health and Reproduction; School of Veterinary Medicine, University of California, Davis, Davis, CA 95616*

[b] *Wildlife Ecology Institute, Starkville, MS 39760*

June 30, 2017

Distribution and Genetic Structure of Sierra Nevada red fox in Oregon

Cate B. Quinn, Tim L. Hiller, Benjamin N. Sacks

Table of Contents

Acknowledgments

We thank many collaborators for contributing occurrence data and genetic samples: J. Akins (Cascade Carnivore Project), J. Doerr , C. Ferland, & R. Seitz (Willamette National Forest), L. Turner & M. Gregg (Deschutes National Forest), S. Colyer, J. VonKienast, & D. Clayton (Rogue River-Siskiyou National Forest), A. Dyck (Mt. Hood National Forest), J. Chapman (Region 6 US Forest Service), J. Nelson (High Desert Museum), S. Mohren & M. Immel (Crater Lake National Park), C. Heath, L. Erickson (Oregon Department of Fish and Wildlife), D. Gumtow-Farrior (Oregon State University-Cascades), G. Green, P. Alden, J. and MacFadden. Funding for this research was provided by Oregon Department of Fish and Wildlife (Agreement 379-15) through a Pittman Robertson grant, along with additional funding and support from the USDA Forest Service, National Park Service, Cascade Carnivore Project, Cascadia Wild, and the Mammalian Ecology and Conservation Unit of the Veterinary Genetics Laboratory in the UC Davis School of Veterinary Medicine.

Executive Summary

The Sierra Nevada red fox (SNRF; *Vulpes vulpes necator*) is native to the subalpine regions of the Sierra Nevada and Cascade mountain ranges of California and Oregon. In the last century, the SNRF has experienced a major range contraction and decline in California, whereas the number, size, and connectivity of populations in Oregon remain unclear. The uncertain status of SNRF in Oregon has impeded monitoring and formation of a conservation strategy for the subspecies. Objectives in this study were to provide an initial characterization of the potential geographic range, effective population size, connectivity, and genetic distinctiveness of SNRF in the Oregon Cascade Range.

We used occurrence records of red foxes in conjunction with environmental covariates to predict the potential SNRF distribution in the Oregon Cascades using maximum entropy (Maxent) modeling. We assembled occurrence records of red fox in the Oregon Cascades from 1985–2016, and subsetted records to independently model an inclusive dataset that employed all available records (n = 169), including unverified visual sightings, and a high-reliability dataset containing only genetic and digital images (n = 124). Two variables, minimum January temperature and land-cover type, were most influential in the model. Models predicted a core distribution along the high-elevation portion of the crest, covering ~3,470 km^2 or 6% of the Cascade region. With the exception of a gap immediately south of Mount Hood, this predicted core distribution was continuous along the north-south extent of the crest, suggesting potentially high connectivity among known occurrence regions.

To assess connectivity among SNRF within the Oregon Cascade Range directly, we analyzed genetic samples. In total, we analyzed 389 genetic samples (hair, scat, tissue) collected in and adjacent to the Cascade region during 2010–2016. Of these, 78 samples were from red fox, and 42 possessed sufficient nuclear DNA to construct individual sex-specific genotypes from 31 microsatellite loci, resulting in identification of 22 distinct individuals. Analyses of maternal, paternal, and bi-parentally inherited markers indicated the occurrence of two distinct populations in the Oregon Cascade. Analysis of population structure indicated a geographic break approximately mid-range, coincident with U.S. Route 20 west of Bend, in an area where Maxent modeling indicated high potential connectivity. Genetic characteristics of the cluster in the southern Cascades were consistent with a small, historically isolated population. Genetic diversity was low (He = 0.44), and the genetic effective population size estimated at the equivalent of 14 breeding adults (95% CI = 11–20).

To assess the genetic distinctiveness of Oregon Cascade populations relative to the Lassen, California SNRF population to the south and Rocky Mountain red foxes (*V. v. macroura*) to the east, we employed admixture and principal component analyses. These analyses indicated the southern Oregon Cascade cluster to be distinct from all neighboring populations, showing no evidence of recent connectivity to Lassen (F_{ST} = 0.34) or other populations outside the Oregon Cascades. In contrast, the population in the northern Cascades had high genetic diversity (He = 0.71), a larger effective population size, equivalent to 48 breeding adults (95% CI = 37–67), and was not significantly differentiated from the Rocky Mountain subspecies (F_{ST} = 0.04). Together, findings suggest that the southern Oregon SNRF population, like those in California, has suffered a severe decline since historical times. However, the norther Oregon SNRF population appears to be connected by recent or ongoing gene flow to the Rocky Mountain subspecies, with the most likely conduit being through the Blue Mountain ecoregion in the northeast portion of the state. Reference samples of nonnative populations (ultimately from fur farms) and Rocky Mountain red foxes from their native range in northeastern Oregon are necessary to clarify the origins of the population in the northern Cascades.

Evidence of introgression from nonnative red fox was limited to 3 individuals on Mount Hood that

carried known fur-farm mitochondrial haplotypes (G-38). The likely immediate source of this introgression was the adjacent low-elevation habitats of the Columbia River Gorge and Interstate Highway 84 (I-84) corridor. However it is unclear whether nearby low-elevation foxes carrying G-38 haplotypes are truly nonnative or whether they are expanding Rocky Mountain red foxes that reflect a small amount of nonnative introgression.

We recommend prioritizing conservation of Sierra Nevada red fox in the southern portion of the Cascades, as red fox in this region appear to be most vulnerable and to represent the most pristine remnant of SNRF ancestry of the Oregon Cascades. However, range-wide occupancy and genetic surveys of the potential distribution identified in this study are needed to determine the current distribution, abundance, home range size, survival, recruitment, and density. Additional genetic sampling is needed, in particular, to facilitate comparison of red foxes in the northern Cascades to reference samples of fur-farm founded populations and endemic Rocky Mountain populations within Oregon.

Disclaimer:

This report was produced in fulfillment of Oregon Department of Fish and Wildlife Agreement No. 379-15 with the University of California, Davis, and was intended to serve as a tentative synopsis of research findings. However, future peer-reviewed publications stemming from this study will supersede this report.

Introduction

The Sierra Nevada red fox (SNRF; *Vulpes vulpes necator*) is one of three subspecies of montane red fox that are endemic to the mountain ranges of western North America. Historically, SNRF occurred throughout the Pacific Crest mountain ranges of California and Oregon (Bailey 1936, Grinnell et al. 1937). During the 20th century, SNRF populations in California declined precipitously. At present, only two known populations occur in California with total numbers estimated to be <50 individuals (Quinn and Sacks 2014, Sacks et al. 2015); currently little information exists on the status and distribution of SNRF in Oregon (Hiller et al. 2015).

The SNRF is currently listed as a state Threatened Species in California, a USDA Forest Service Sensitive species in the Intermountain (R4), Pacific Southwest (R5), and Pacific Northwest (R6) regions, and a Strategy Species in the Oregon Conservation Strategy (2015). In 2011, the subspecies was petitioned for listing throughout its range under the US Endangered Species Act. Following a 12-month review, the United States Fish and Wildlife Serviced determined in 2015 that the SNRF population in the Sierra Nevada warranted listing as a distinct population segment (DPS; precluded by higher priorities), but declined to recommend listing for the Lassen or Oregon populations, which were grouped together in a single Southern Cascades DPS (U.S. Fish and Wildlife Service 2015a,b).

The decision to treat southern Cascades populations of California and Oregon as a single DPS and not to recommend listing was based on of the absence of information regarding the current status of SNRF in Oregon as well as their presumed connectivity to the Lassen population (U.S. Fish and Wildlife Service 2015b). A genetic study using historical museum SNRF specimens found that by mid-century, samples from the southern Cascades (including Lassen, Shasta [now presumed extirpated], and Oregon) were already somewhat isolated from those from the Sierra Nevada mountains to the south (Sacks et al. 2010). Modern samples collected from the two remaining California populations in the California Cascades (Lassen) and the Sierra Nevada (Sonora Pass) indicated a complete lack of contemporary gene flow (Statham et al. 2012a). Until recently, no modern samples from Oregon have been available to assess the connectivity between the populations in southern Oregon and Lassen that make up the Southern Cascades DPS.

Over the past 6 years, agencies and organizations have accumulated georeferenced reports, photographs, and genetically identified samples collected incidentally or during surveys for SNRF or other forest carnivores (e.g., Hiller et al. 2015). These recent detections were consistent with the elevation and habitat profile of the historical population and have spurred optimism that SNRF could be more plentiful in the Oregon Cascades than in the southern part of their range in California (U.S. Fish and Wildlife Service 2015b). Detections ranged as far north as Mount Hood and as far south as Crater Lake National Park. These detections clustered into sighting areas separated by 50–100 km (U.S. Fish and Wildlife Service 2015a). Whether these occurrences represented isolated populations of individuals or a single, continuously distributed but poorly sampled population, was unclear. Few museum or other records exist to provide a historical baseline of the distribution, density, and connectivity of SNRF in Oregon, although natural history accounts agree that SNRF were generally concentrated in the park-like mosaic of open subalpine forests and wet meadows in the high-elevation (>1,219 m) portions of the Cascade Range (Bailey 1936, Ingles 1965, Aubry 1983, Verts and Carraway 1998).

The occurrence of another native montane subspecies, as well as nonnative red foxes, in Oregon also necessitates assessing the genetic integrity of SNRF. The Rocky Mountain red fox (*V. v. macroura*), which historically occurred in the Blue Mountain and Wallowa Ranges in the northeastern corner of the state (Bailey 1936; Aubry et al. 2009), has recently increased in abundance and broadened its range to include

lower elevation habitats, such as cultivated farmland (Green et al., in press). Additionally, fur farms in Oregon started utilizing nonnative red foxes during the 20th century (Verts and Carraway 1998) and individuals were known to have escaped or been released from captivity. Although nonnative red foxes typically occur in close proximity to humans in urban and disturbed landscapes (Statham et al. 2012b, Sacks et al. 2016, Merson et al. 2017), they can interbreed with native populations where they come into contact. Consequently, nonnative fur-farm genes have introgressed into multiple native red fox populations throughout the western U.S. (e.g., Sacks et al. 2011; Quinn and Sacks 2014; Merson et al. 2017; Green et al., in press).

Our objectives in this study were to provide an initial characterization of the potential range, effective population size, connectivity, and genetic distinctiveness of SNRF in the Oregon Cascade Range. We used two complimentary approaches to meet our objectives. First, we used occurrence records of red foxes in conjunction with environmental covariates to develop a predictive model of potential SNRF distribution in the Oregon Cascades. This model was produced to guide future survey efforts as well as to provide a spatially explicit context for mapping genetic connectivity within Oregon. We modeled the distribution in a maximum entropy framework using Maxent software (Phillips et al. 2006, Phillips and Dudík 2008). Second, we analyzed genetic samples collected in and adjacent to the Cascades using a combination of maternally, paternally, and bi-parentally inherited genetic markers. We analyzed genetic samples for evidence of substructure within the Cascades, and estimated genetic effective population size and diversity within and pooled across subpopulations. We additionally investigated contemporary genetic connectivity of Oregon SNRF to neighboring montane populations using previously published reference data.

Methods

Field Data Collection

In collaboration with biologists from multiple state and federal agencies and non-governmental organizations, we amassed red fox genetic samples collected during 2012–2016 (n = 78; Table 1; Fig. 1) along with photographically documented (Fig. 1) and unverified red fox sightings during 1985–2016 (n = 97; Appendix 1), from Deschutes, Mount Hood, Umpqua, and Willamette National Forests, and Crater Lake National Park, which collectively encompass the majority of potential SNRF habitat within Oregon. These samples and records (n = 175) were derived opportunistically and from targeted surveys that varied in intensity, duration, and coverage. Methodologies included ad hoc and systematic baited camera surveys (Hiller et al. 2015), scat searches and hair snares, opportunistic visual sightings, and a small number of road-killed foxes. Fecal samples were stored in 95% ethanol; hair and tissue were stored in desiccant until DNA extraction and species identification (see ***Laboratory Analyses***).

Species Distribution Modeling

We modeled species distribution in Maxent version 3.2.1 (Phillips et al. 2006), chosen for its flexibility in use of presence-only data and robustness to small sample sizes (Hernandez et al. 2006, Wisz et al. 2008). As with other approaches to modeling species distributions, Maxent uses statistical associations between occurrence localities and environmental correlates to project regions in environmental space similar to detection sites.

Occurrence Records — We considered only samples that fell within the East Cascades or West Cascades ecoregions, as defined by the Oregon Conservation Strategy (2016), which led to exclusion of 6 genetic samples east or north of these ecoregions. The different types of data available for analyses likely entailed

different biases with unknowable effects on distribution models. In particular, reliance solely on the most reliable presence data (digital images, genetic detections) entailed greater spatial bias as surveys collectively reflected a relatively small portion of the available landscape. Conversely, sightings, which represented opportunistic sampling of a comparably large fraction of the landscape, were more vulnerable to false positives. Therefore, we built models based on two datasets and considered the extent of model agreement to be an indicator of model robustness and, to the extent that they disagreed, considered each to reflect an opposite end of a range of potential distributions. The confirmed occurrence dataset (n = 124) included digital images (n = 52) and genetic detections (n = 72) recently collected (2010–2016), whereas the inclusive dataset (n = 169) was composed of the same 124 records plus another 45 records of unverified sightings spanning a greater interval of time (1985–2016). To reduce pseudoreplication owing to spatially nonrandom sampling, we filtered occurrence records to retain only one record in a 4-km^2 neighborhood (Boria et al. 2014), which provided a reasonable balance between spatial independence and sample size. The filtered dataset resulted in 33 occurrences for the confirmed data set and 62 occurrences for the high-inclusivity dataset.

Spatial extent and background points — Maxent models are sensitive to the spatial extent of available habitat (background) used for model training (Lobo et al. 2008, Elith et al. 2011). To limit model training to areas more likely to have been surveyed, we restricted background extent to the vicinity of occurrence localities. Specifically, for each dataset (i.e., confirmed, inclusive) we buffered occurrence points using a 20-km radius and randomly sampled a total of 10,000 points within the cumulative buffered area for use as background points in model development. The distribution of genetic samples from non-target species (which were not used in modeling) provided an approximate sense of the survey area beyond our SNRF detections, which corresponded well to the 20-km buffer distance (Fig. 1). We then projected distribution models to the entirety of both Oregon Cascades ecoregions (hereafter, the "Cascades ecoregion").

Environmental Variables — We initially assembled 29 environmental layers to characterize aspects of climate, topography, and vegetation across the available landscape (Appendix 3). We extracted 14 bioclimatic variables from the WorldClim database (Hijmans et al. 2005) derived from temperature and precipitation. We substituted 5 WorldClim values (BIO1, BIO5, BIO6, BIO12, BIO 19) for corresponding climate data from the Parameter-elevation Regressions on Independent Slopes Model (PRISM; Daly et al. 1994). PRISM is another climate model that uses point data and digital elevation models to generate gridded estimates, and has been shown to perform well in mountainous terrain (Daly et al. 1994). Specifically, we used 30-year normal data sets to extract layers of annual precipitation totals and temperature extremes, as well as monthly estimates for winter (Dec.– Feb.) and summer (June–Aug.) seasons.

We derived 3 topographic layers from the US Geological Survey 1 arc-second global digital elevation model. We used the terrain function in R package raster (Hijmans 2016) to calculate slope, roughness (the difference between the maximum and minimum elevation value of a cell and its surrounding neighbors), and aspect. We transformed aspect to a continuous variable between 0 and 1 by taking the absolute value of degrees after normalization (McCune et al. 2002, Kalle et al. 2013). This transformed aspect depicts incident radiation, but can be interpreted as "southness" as the value approaches 0 at northerly aspects and 1 at southerly aspects.

We used 2 variable sets to characterize vegetation type and vertical structure. We obtained vegetation land-cover layers from the Northwest ReGAP Ecological System (2010; http://inr.oregonstate.edu/existing-vegetation), a national project that uses 30-m Landsat satellite data to map ecological land-cover classes (http://gapanalysis.usgs.gov). We adjusted existing land-cover categories to group agriculture and development into a single "disturbed" category, and we lumped

"Siskiyou Mixed Conifer Forests and Woodlands" with "Mixed Conifer Forests" (Appendix 3). Additionally, we used percent canopy cover to characterize density at a finer scale within forest types (LEMMA GNN https://lemma.forestry.oregonstate.edu/data/structure-maps).

After assembling and resampling all layers to a resolution of 30 arc-seconds (~0.83 km^2), we reduced the full suite of variables to the least correlated subset to encourage simpler, more interpretable models (Dormann et al. 2013). Using the vif.cor function in R package usdm (Naimi 2015), we identified the pair with the highest linear correlation, and excluded the variable that possessed the highest variance inflation factor (VIF), an index of collinearity derived from regressing the predictor variable against all other variables. We iterated this process until all remaining variables had a pairwise correlation below a threshold of 0.7. After pruning for collinearity, we conducted no further selection of variables prior to modeling, but allowed the internal regularization function within the Maxent algorithm to select the most informative variable transformations.

Finally, as a heuristic check on modeled relationships, we investigated the relationships between the raw occurrence data and range of environmental conditions available on the study area. We created selection indices log-transforming the ratio of observed to expected proportion of occurrence records (+1 to avoid division by zero), and subtracting log(2) so that positive and negative values corresponded to greater and less use relative to expectations, respectively (e.g. Neale and Sacks 2001). We visually inspected selection indices for evidence of strong relationships (e.g. linear, quadratic) between red fox occurrence and environmental conditions, and compared these to functional forms modeled by Maxent. We also qualitatively compared the identity of the variables with the strongest relationships to their percent contribution, a path-dependent proxy for variable importance calculated during the Maxent fitting process.

Modeling —Maxent limits model complexity internally through regularization. Similar to the lasso technique used in generalized linear models, regularization adds a penalty term to each non-linear transformation of an environmental variable (i.e. feature), effectively shrinking model coefficients toward zero (Merow et al. 2013). Higher regularization thus minimizes the number and functional forms that transformations can take, resulting in simpler models with fewer parameters. Simultaneously, regularization relaxes the constraint that the environmental covariates associated with the predicted distribution empirically match those of the occurrence data; as a result, higher regularization values also tend to generate smoother, more uniform probability distributions.

Regularization coefficients in Maxent are individually preset for each feature class (e.g. linear, quadratic, product), but users can adjust the strength of all penalties simultaneously through use of a multiplier constant (referred to hereafter as β). Phillips et al. (2006) suggested the default setting ($\beta = 1$) is sufficient for multi-species modeling, but more recent work strongly advocates species-specific tuning of this multiplier (e.g., Warren and Seifert 2011, Shcheglovitova and Anderson 2013, Radosavljevic and Anderson 2014). Optimizing regularization for a given study system has been shown to prevent overfitting and improve prediction accuracy (Shcheglovitova and Anderson 2013, Radosavljevic and Anderson 2014), particularly for models built from small numbers of geographically biased records (Anderson and Gonzalez 2011).

To identify optimal levels of model complexity, we built models in the R package ENMeval (Muscarella et al. 2014) for each dataset using a range of values for the regularization multiplier ($\beta = 0.5–6$ in increments of 0.5), and considered only linear, quadratic, and product feature classes (transformations). We selected the optimal regularization setting based on the model's ability to predict data withheld from model training. Spatial correlation among training and testing data consistently overestimate model performance, as presence points close in geographic space are typically close in environmental space

(Hijmans 2012, Radosavljevic and Anderson 2014). As a result, evaluation metrics are especially misleading when occurrence points are clustered. We opted instead to manually partition presence and background points into spatially independent folds for cross-validation, using latitude to split points into three bins (i.e., spatial folds) of equal sample size (latitudes for sightings: Bin A, <43.150; Bin B, 43.150–43.987; Bin C, >43.987; latitudes for confirmed: Bin A, <43.600; Bin B, 43.600–44.194; Bin C, >44.194). Each modeling iteration was trained using two of three partitions while the third partition was withheld for model evaluation.

We assessed relative overfitting using the average area under the receiver operating curve (AUC) value of the held-out partition (AUC_{TEST}) and the difference between training and test AUC values (AUC_{DIFF}). The AUC indicates how well the model correctly ranks test presence points above background points (Phillips et al. 2006), and serves as a threshold-independent indicator of a model's ability to discriminate between low and high probabilities of occurrence. With presence-only data, AUC treats background points as absences, which can create misleading evaluations when used as an absolute indication of model quality for species like SNRF with low prevalence and low sampling effort (Lobo et al. 2008, Peterson et al. 2008, Bean et al. 2012, Merow et al. 2013) Here, we used AUC to rank models built from the same datasets with differing levels of complexity. We chose selected optimal regularization settings by balancing gains in average test AUC (AUC_{TEST}; predictive power) with increases in the difference between test and training AUC (AUC_{DIFF}; overfitting). To allow comparison between spatial folds, we trained models using the spatially binned background points described above, but calculated AUC values using the full set of background points.

Optimal regularization settings were applied to the final models, which were then parameterized using the entire dataset. We transformed raw predictions using the logistic transformation for visualization purposes and comparison among models, but treated these values as ordinal indexes of the probability of occurrence as opposed to true probabilities of occurrence (Yackulic et al. 2013).

Finally, we used two levels of model thresholds for the purposes of qualitatively comparing models and stratifying the landscape for future surveys. Thresholding decisions always entail some degree of arbitrariness, and some of the most commonly used approaches (e.g. lowest presence threshold) are sensitive to small sample size (Loiselle et al. 2003, Bean et al. 2012). We decided thresholds for the most restrictive model using an approach that attempts to balance sensitivity and specificity (Engler et al. 2004), and then applied these criteria uniformly to the other models to allow comparison. Specifically, we chose threshold values that maximized the difference between the proportion of presence sites versus the proportion of the study area where presence was predicted, i.e., maximizing the model's discriminatory power.

Genetic Structure and Diversity

Laboratory Analyses

We conducted DNA extraction, PCR amplification, sequencing, and genotyping at the Mammalian Ecology and Conservation Unit of the Veterinary Genetics Laboratory at the University of California, Davis. We extracted DNA from feces (n = 362) using QIAamp (R) Stool Kit, and from hair (n = 24) and tissue (n = 3) using DNeasy Blood and Tissue Kits (Qiagen Inc., Valencia CA). For fecal and tissue samples, we followed manufacturer's instructions for the corresponding kit. For hair samples, we modified the manufacturer's protocol by digesting a 0.5–1 cm length of hair, including the follicle, from 1–20 hairs to 300 µl Buffer ATL, 20 µl proteinase K, and 20 µl 1M DTT; subsequent steps followed manufacturer's protocol. To prevent and detect contamination, we extracted DNA from feces and hair

with negative controls on a bench dedicated to low-quantity DNA.

Overview of molecular markers — We used several types of genetic marker. We used DNA sequences from the mitochondrial genome (mtDNA) to identify species and, for red fox, to assess origin of maternal ancestry. We used a marker associated with Amelogenin gene paralogs on X and Y chromosomes to identify sex of foxes. For males, we used Y chromosome microsatellites to assess the paternal line. For all foxes, we used autosomal nuclear microsatellites (31 loci) to determine individual identity, familial relationships, genetic diversity, and population identity and connectivity.

Because of our use of noninvasive samples, we obtained multiple samples for some individuals. Therefore, for efficiency, we performed analyses in the following order: (1) sequence of mtDNA at 354 bp of cytochrome b gene (cyt b) to determine species, (2) genotype autosomal microsatellites and sex-marker to determine individual (and sex), (3) sequence 343 bp of the mtDNA D loop region (one sample per individual) and, for a subset of these samples, (4) sequence 200 additional bases of the cytochrome b gene; lastly, (5) we genotyped one sample for each individual male at the Y chromosome microsatellites. Below, the technical specifics of the sequencing and genotyping are described.

MtDNA — We attempted to sequence all samples at the 354-bp portion of the cyt b locus of the mtDNA using previously published primers (RF14721, RF15149; Perrine et al. 2007). To sequence the 343-bp portion of the D Loop, we used primers VVDL1, VVDL6 (Aubry et al. 2009) and concatenated it with the 354-bp cyt b fragment for comparison with a growing database of previously published haplotypes (Aubry et al. 2009, Statham et al. 2014, many others). The nomenclature for these concatenated haplotypes followed previous studies; specifically, the cyt b fragment was indicated by a letter or letter-numeral combination before a dash and the D loop fragment was indicated by a numerical reference after the dash, e.g., 'A-19.' Because haplotype A-19 is a widespread haplotype ancestral to all other haplotypes within the mountain subclade (see ***Data Analyses***), we further resolved A-19 haplotypes by sequencing at an additional 200 bp of the cytochrome *b* gene (primers VVmc-780F and VVmc-980R; Volkmann et al. 2015). These primers amplified a SNP at bp-position 889 discovered by Volkmann et al. (2015) that divides haplotype A-19 into two subhaplotypes distinguished by ≥7 mutations in the broader mitochondrial genome (Figs 2A, 3 in Volkmann et al. 2015). For all sequencing reactions we used methods, reagents, and thermal-cycling conditions described previously (Perrine et al. 2007, Aubry et al. 2009, Volkmann et al. 2015).

Nuclear Microsatellites — We genotyped red fox samples at 31 microsatellites (AHT121, AHT137, C04.140, FH2004, FH2289, Vv-V142, V402, V468, V602, Vv-AHTh171, Vv-C01.424, Vv-C08.618, Vv-CPH11, Vv-CPH18, Vv-CPH2, Vv-CPH3, Vv-CXX-279, Vv-FH2001, Vv-FH2010, Vv-FH2054, Vv-FH2088, Vv-FH2328, Vv-FH2380, Vv-FH2457, Vv-FH 2848, Vv-INU030, Vv-INU055, Vv-REN105L03, Vv-REN 162C04, Vv-REN169O18, Vv-REN247M23, Vv-REN54 P11) and a sex marker, K9-AMELO (Wandeler and Funk 2006, Moore et al. 2010). We conducted PCRs in five multiplex groups (Moore et al. 2010) using the Qiagen multiplex kit with Q-solution and thermal profile recommended in the manufacturer's protocol, with an annealing temperature of 58 °C. We electrophoresed PCR products on an ABI 3730 capillary sequencer (Applied Biosystems, Foster City, CA, USA) and scored alleles relative to an internal size standard, Genescan 500 LIZ (Applied Biosystems) in program STRand (Toonen and Hughes 2001). We replicated all genotypes 2 to 8 times to detect false alleles and correct for allelic dropout, and excluded genotypes from downstream analyses that were missing alleles at ≥3 loci.

Y-microsatellites — We genotyped 12 microsatellites located on the Y-chromosome for distinct individuals using the same procedures outlined above (VVY10, VVY11, VVY13, VVY14, VVY16, VVY17, VVY3, VVY5, VVY7, VVY8, Y29, Y30; Statham et al. 2014; Rando et al., in review). As the Y-chromosome does not undergo recombination, we allowed for incomplete haplotypes (>7 loci amplified)

and imputed missing alleles. This approach is conservative in that it may fail to detect new haplotypes, but can be used to exclude previously sampled haplotypes and provide minimum estimates of patrilineal diversity.

Data Analyses

Species typing, individual identification, and familial relationships— We used the Basic Local Alignment Search Tool (BLAST; Altschul et al. 1990) in conjunction with cyt b haplotypes to search for homologous sequences in Genbank. For samples identified as red fox (based on ≥98% sequence homology), we then identified them to individual of a particular sex as follows: Genotypes that matched at >85% of loci in AlleleMatch (Galpern et al. 2012) were assumed to be the same individual and consolidated to create a consensus genotype. We identified family groups that could skew tests of genetic differentiation using an exclusion-based parentage analysis in Cervus (allowing for up to two trio mismatches) (Kalinowski et al. 2007), and conservatively assuming that individuals sampled from the same sighting region and sharing >55% of alleles were first-order relatives.

Population structure within the Oregon Cascades — We used a Bayesian clustering algorithm to group individuals according to their autosomal microsatellite genotypes in Structure v. 2.3.4, using the admixture model with correlated allele frequencies and no prior information (Pritchard et al. 2000, Falush et al. 2003). First, to determine the appropriate number of genetic clusters (K), we ran 10 independent iterations at K = 1–8 for 30,000 MCMC repetitions, discarding the first 10,000 as burn-in. We implemented two methods to select the appropriate K value in Structure Harvester (Earl 2012): one that maximizes the log probability of the data (Pritchard et al. 2000) and a second based on the rate of change of the log probability of the data between successive iterations (delta-K method; Evanno et al. 2005). We performed a final run at the indicated number of clusters (K) using 1,100,100 MCMC cycles, discarding the first 100,000 as burn-in, and used these estimated proportion of ancestry (q) to assign individuals to populations. Finally, because closely related individuals can artificially create the appearance of substructure with a small number of samples, we performed an additional run of the above analyses on a subset of individuals that excluded putative first-order relatives.

Maternal and paternal ancestry—The shared ancestry of all montane subspecies prevented determination of whether a maternal haplotype (e.g., A-19) was endemic to the Oregon Cascades or originated in another montane population. However, we could use mitochondrial haplotypes to differentiate native from nonnative maternal ancestries. Populations founded from nonnative fur-farm foxes share a common set of haplotypes throughout the US (Statham et al. 2012b, Kasprowicz et al. 2016, Sacks et al. 2016, Merson et al. 2017), and because breeding stock was traded originally from Alaska and eastern Canada (Balcom 1916, Laut 1921), these haplotypes are distinct from native montane haplotypes (Aubry et al. 2009). The only montane haplotype that has also been used in fur farms and observed in nonnative populations is O-24, a haplotype historically found only in the Washington Cascades (Sacks et al. 2010; Lounsberry et al. 2017). We therefore considered any haplotype previously sampled in fur-farms, or originating from the Eastern or Alaskan clades, as indicative of past gene flow with fur-farm-derived foxes. The Y-chromosome markers were only recently developed (Rando et al., in review). Therefore, we did not have sufficient reference data to assign Y microsatellite haplotypes to a particular geographic origin. However, Y markers served as indicators of patrilineal genetic diversity and population structure.

Genetic Diversity— We estimated indices of genetic diversity for the total sample and for samples corresponding to discrete populations identified in program Structure. We tested for departure from Hardy-Weinberg proportions (F_{IS}) across loci in FSTAT v. 2.9.3 (Goudet 2001). We assessed significance by comparing the observed value to random permutations of alleles within samples, after adjusting for multiple tests using sequential Bonferroni correction (Rice 1989). We estimated observed heterozygosity

(H_o) and expected heterozygosity (H_e, i.e., under Hardy Weinberg equilibrium) in Microsoft Toolkit (Park 2001), and allelic richness in FSTAT. We estimated the genetic effective population size (N_e) of each population based on the decay of linkage equilibrium in LDNE (Waples 2006, Waples and Do 2008), excluding alleles with frequencies <0.02 and using jackknife-based confidence intervals. For each population, we estimated N_e under the assumption of monogamy and random-mating.

Connectivity to other montane populations — We used three independent approaches to assess the relationship of populations in the Oregon Cascades to other montane subspecies. First, we used the model-based Structure algorithm to assess how Oregon samples clustered with previously published (Sacks et al. 2010) autosomal microsatellite genotypes at the same 31 loci from the contemporary Lassen population in northern California (*V.v. necato*r; n = 12), the Washington Cascades (*V.v. cascadensis*; n = 5), and the Rocky Mountains in Idaho, Colorado, Wyoming, and Nevada (*V.v. macroura*; n = 22). We used the methodology outlined above to determine the optimal number of clusters, but because we were interested in assessing the relationships among groups (versus assignment to pre-defined populations), we evaluated Structure results at multiple K-values.

Second, to support Structure results and visualize the relationships among individuals with no assumptions about Hardy-Weinberg or linkage equilibria, we subjected the same group of montane samples to a multivariate distance-based approach. Specifically, we used principal components analysis (PCA) to summarize the variability in microsatellite allele frequencies among individuals in R package adegenet (Jombart 2008), which provided an indication of the relative dissimilarity among groups in two-dimensional space. Lastly, we computed pairwise estimates of F_{ST}, a commonly reported measure of genetic distance, in FSTAT.

Results

Based on 169 detections (genetic samples, photographs, sighting reports; 1985–2016), red fox occurrence was nonrandomly associated with land-cover type and minimum January temperature (Fig. 2). Montane meadows, silver fir and mountain hemlock forests, subalpine woodlands, and alpine habitats all had more observed red fox detections than expected based on the composition of available habitat. In contrast, although disturbed land-cover types, mixed conifer forest, and ponderosa pine together accounted for 40% of red fox presence points, red foxes were observed less frequently in these land-cover types than expected. Red fox occurrence was disproportionately concentrated in locations with intermediate minimum January temperatures, specifically in the range, -7.5 to -4.5 °C. No clear selection trends were apparent relative to other environmental gradients (Appendix 4).

Species Distribution Modeling

After filtering variables based on VIF, the final 9 variables subjected to modeling were minimum temperature in January, total precipitation in December, precipitation seasonality (standard deviation of precipitation), temperature seasonality (standard deviation of temperature), isothermality, transformed aspect, roughness, percent canopy cover, and land-cover type. Based on 124 confirmed detections (genetic samples [see below], digital images; 2010–2016) or 169 inclusive detections (verified detections, 2010–2016 plus unverified sighting reports, 1985–2016), land-cover type and minimum January temperature were the highest contributing variables in all Maxent models, together accounting for 75–90% contribution across final models (Table 2). Meadows consistently had large positive coefficients (λ) in all Maxent models, while other land-cover variables positively influenced the probability of red fox occurrence but varied in strength depending on regularization (Appendix 5). Higher minimum January temperatures exhibited a strong negative influence on the probability of occurrence in all models.

In both datasets, intermediate regularization settings improved predictions of spatially independent data

(Table 3; Fig. 3). We selected optimal regularization values at the point where increasing regularization no longer exhibited significant rates of change in AUC_{TEST} and AUC_{DIFF} ($\beta = 3$ for confirmed; $\beta = 2.5$ for inclusive). Optimizing regularization effectively reduced the number of parameters from 15 to 7 in the confirmed dataset, and 19 to 11 in the inclusive dataset. Across all settings, the confirmed dataset showed higher variability of performance among spatial folds, as well as larger AUC_{DIFF} values, suggesting an overall greater statistical vulnerability to overfitting (Fig. 3).

Visual inspection of model projections over a range of regularization settings consistently revealed a narrow longitudinal strip along the Cascade crest as the region with the highest probability of occurrence (Fig. 4). In contrast, occurrence probabilities for the eastern slope of the Cascades were highly sensitive to regularization, but, in general, rarely exceeded intermediate values.

To dichotomize the model, we chose threshold probability values from the confirmed dataset with default regularization, as it resulted in the most restricted distribution. We identified two clear maxima in the difference between the proportion of study area and the proportion of fox points included in the predicted area (Appendix 6). The lower threshold (0.27) yielded a more permissive threshold that predicted 12% of Cascades ecoregion as potential range (35% of buffered background points) and correctly assigned 91% of confirmed red fox points (Table 4). The more restrictive probability threshold (0.50) assigned 4% of the Cascade ecoregion (16% of buffered background points) as predicted habitat and resulted in 73% of the confirmed red fox localities correctly predicted. When the more restrictive threshold was applied across all models, on average 6% (3,470 km^2 SD 846 km^2) of the Cascades ecoregion was predicted as high probability of presence (Table 4). The models built from the inclusive dataset that included sightings predicted a larger potential range than the confirmed dataset at both threshold decisions (Table 4).

Genetic Structure and Diversity

Species typing, individual identification, and familial relationships — We successfully amplified cyt b sequences from 310 of 389 samples (80%), yielding 78 samples species-typed as red fox and 232 non-target species (Table 5). Of these, 42 (54%) samples amplified a sufficient number of microsatellite loci to provide usable genotypes, resulting in 22 individual red foxes (Table 1). Seventeen individuals sampled along the Cascade crest clustered into four regions: Mount Hood (n = 4), a 50-km stretch centered on the Three Sisters (n = 4), a tight cluster around Willamette Pass (n = 5), and Crater Lake National Park (n = 4) (Fig. 6). Four individuals were sampled adjacent to the Cascades ecoregion in human-settled areas not typically associated with Sierra Nevada red fox (Hood River: n = 1; Bend n = 4). Finally, one individual was incidentally sampled from Malheur County and assumed a priori to be either a nonnative fur-farm or Rocky Mountain red fox (e.g., Green et al., in press).

Seven individuals were sampled multiple times (range = 2–7 detections), with inter-individual distances ≤9.4 km (Fig. 6). Based on parentage analyses, we identified a mated pair and 2 offspring sampled in 2014 from the Willamette Pass area. Additionally, 2 hair samples collected near a den outside of Bend showed allele-sharing consistent with full sibling-ship.

Maternal and paternal ancestry — Among the 22 individuals identified based on microsatellite genotypes, 18 possessed A-19 maternal haplotypes and 4 possessed G-38 haplotypes (Table 6). The G-38 haplotypes were found in 3 individuals on Mount Hood and one individual outside Hood River. Of the 31 samples that could not be assigned to individual based on microsatellite genotypes, 25 were A-19 (including 21 complete sequences, 4 partial sequences), and 4 were G-38. These G-38 samples also were collected on Mount Hood, near the individually genotyped samples with G-38 haplotypes.

Additional targeted sequencing demonstrated a geographic break within A-19 samples along the north-south axis of the Cascade Range (Fig. 8b). The A-19 haplotypes south of U.S. Route 20 and west of Bend

(n = 12) exhibited subhaplotypes that corresponded to *w1*, *w2*, or *w3* in Volkmann et al. (2015), hereafter collectively referred to as A-19a, and haplotypes north and west (n = 5) corresponded to haplotypes *w6*, *w7*, or *w8*, hereafter collectively referred to as A-19b. Both subhaplotypes had been previously sampled in museum specimens (Volkmann et al 2015).

Nine of 12 males (75%) amplified >7 microsatellite loci on the Y chromosome, yielding 4 paternal haplotypes (Table 6). All individuals south of U.S. Route 20 (mentioned strictly as a convenient landmark) carried a single paternal haplotype (n = 5), whereas the 4 individuals sampled near Bend and Mount Hood possessed 3 distinct haplotypes (the 2 individuals with shared haplotypes were putative siblings from Bend) (Fig. 8c).

Population structure within the Oregon Cascades — Bayesian structure analyses conducted within the Oregon Cascades using autosomal microsatellite genotypes indicated strong support for genetic clusters geographically segregated into northern and southern groups, with a geographic break that mirrored the discontinuity in mitochondrial markers and Y chromosome, i.e., corresponding approximately to U.S. Route 20 (Fig. 7, 8). ($q > 0.9$), with the exception of three individuals sampled near U.S. Route 20 that showed proportion of ancestry intermediate between the two groups. Notably, one individual sampled from Crater Lake National Park at the southern extent of the known range strongly assigned to the northern cluster. The sample from Malheur County, 150 km east of the Cascades, also consistently grouped with the northern cluster, even at higher K values. Removing putative first-order relatives from Structure runs had no qualitative influence on assignment of ancestry (data not shown).

Genetic diversity —Tests for Hardy-Weinberg proportions showed a significant excess of heterozygotes relative to expectations when estimated across all samples (Table 7). When individuals were sorted into populations according to their K-values, the northern cluster did not significantly deviate from Hardy-Weinberg proportions and the southern cluster exhibited a significant excess of heterozygotes. The southern cluster possessed markedly lower estimates of nuclear genetic diversity and effective population size relative to the northern population, and were slightly higher but close in magnitude to estimates for the Lassen population.

Relationship to other montane populations — We combined Oregon samples with previously published contemporary samples of montane red foxes from Lassen, Washington, and the Rocky Mountains (Sacks et al. 2010) to characterize clustering over a broader spatial scale. Structure analyses showed strong support for the southern cluster as a distinct population (Fig. 9). The Lassen population was the first to break out at K = 2, followed by the southern Oregon samples at K = 3. At K = 4, the Washington Cascade foxes split into a distinct cluster, which left northern Oregon and the Rocky Mountains as one undifferentiated cluster. Higher K-values caused the Rockies to disaggregate; at no K-value did the northern Oregon samples split as a population distinct from the Rocky Mountains.

The PCA supported the relationships suggested by the Bayesian clustering approach. The first principal component (12.5% variance explained) separated Lassen from the larger group; the second principal component (8.8% variance) separated the southern Oregon samples, and the third principal component (6.4% variance) showed the Washington Cascades as distinct from the Rocky Mountains (Fig 10). The Rocky Mountains and northern Oregon samples overlapped in all three dimensions.

The pairwise genetic distances among southern Oregon and the two California populations were large and similar in magnitude (F_{ST} = 0.34–0.40; Table 8). The lowest pairwise distance among all montane populations occurred between samples from northern Oregon and the Rocky Mountains.

Discussion

Species Distribution Modeling

We combined disparate sources of SNRF detection data to maximize distributional information and generate predictive surfaces of relative probabilities of occurrence for SNRF in the Oregon Cascades. We used thresholds to discretize surfaces to facilitate stratification of survey units into predicted presence, and provided continuous predictions that preserve relative probabilities for use in selection of micro-sites within survey units and quantification of uncertainty. Such predictive layers have the greatest value for rare species when used in an adaptive framework: models enable more efficient survey design, and in turn new detections are fed back into the model to improve accuracy and generality, as each iteration of data collection diminishes geographic bias (Guisan et al. 2006). Maxent predictions also can be used as the basis for designing a comprehensive range-wide presence-absence survey that systematically incorporates predicted-presence and predicted-absence sites to estimate occupancy (e.g., Preckler-Quisquater et al. 2017).

We produced 4 final models that varied in the stringency of input data (confirmed, inclusive) and model complexity (regularization settings). Models differed in the areal extent for predicted presence, with inclusive > confirmed, and higher regularization > default settings. The model with default settings and confirmed data generated the most restrictive prediction with the highest discriminatory power, and the model built from the inclusive dataset that incorporated sighting and higher regularization was the most permissive model, presumably with the greatest generality and least overfitting. We suggest the most permissive (sightings $\beta = 2.5$) is most useful in exploring and expanding range limits, both environmental and geographic, and particularly in surveys of the eastern slope. In turn, the most restrictive model (confirmed $\beta = 1$) with the least high-probability area predicted is best suited for optimizing the detection of new individuals. This model generated the narrowest region of high probability common to all models, and thus while it may exclude occupied regions, it is most likely to maximize the ratio of new detections to survey effort.

The high-elevation zone corresponding closely to the Cascade crest (i.e., that we refer to as the “core” potential SNRF range) constituted high probability habitat according to all models regardless of which dataset or regularization setting was used and was therefore our most robustly supported inference about potential SNRF distribution. Our analysis necessarily included some degree of sampling bias. Sampling bias is most problematic when it excludes environmental variables or combinations. In our case, occurrence localities were clustered close to the crest with little east-west variation, but were well-dispersed in clusters along the north-south axis. Moreover, the buffer size used (20 km) to define our available (background) habitat corresponded well to the distribution of our genetic samples relative to the red fox detections. While it is likely that low sampling effort contributed to intervening gaps in presence data on the latitudinal axis, the environmental space that characterizes the high-elevation portion of the Cascades was generally well-sampled. Maxent was therefore a useful tool to predict regions with environmental traits similar to clusters, regardless of false absences. Furthermore, the division of training and test data into latitudinal bins served to validate our model. Altogether, these findings point to the strip of habitat encompassing the crest to be the highest priority for future surveys to detect new individuals.

The Maxent algorithm has no means to distinguish realized from potential habitat, which is important in predicting ranges of non-equilibrium populations. Notably, all unverified sightings that occurred on the eastern slope were reported prior to the mid-1990s. It is possible that distribution of SNRF was substantially greater in past decades, exhibiting a wider environmental tolerance than is represented by remnant pockets persisting today. For example, Grinnell et al. (1937) indicated SNRF in the Sierra

Nevada range were trapped or observed in mid-elevation forest as low 1,980 m, but today have been detected nearly exclusively above 2,750 m in the central Sierra Nevada (Quinn and Sacks 2014). If contemporary records accurately represent the fragmented nature of SNRF populations in the Oregon Cascades, and if these contractions did not occur randomly in environmental space, the more restrictive models built from recent detections may serve as a more useful representation of contemporary potential habitat.

With respect to landscape connectivity, all models predicted high connectivity along the north-south extent of the crest, with the only notable gap occurring just south of Mount Hood. As discussed below, however, genetic connectivity appeared high across this gap, and less so further south where the model exposed no break in connectivity.

Genetic Structure and Diversity

Substructure — The most striking result from our genetic analyses was the indication that two populations with distinct genetic characteristics occur in the Oregon Cascade Range. Results of mitochondrial, Y-chromosome, and autosomal markers were consistent in the differentiation of individuals sampled from the northern and southern portions of the range with a geographic break coincident with U.S. Route 20 west of Bend. All of the individuals that were assigned to the southern genetic cluster based on microsatellite genotypes carried distinct maternal and, for males, paternal haplotypes, that were not shared with individuals assigned to the northern cluster. All three markers supported that the southern population was small and historically isolated, analogous to the population of SNRF in Lassen, California.

The Maxent model provided little insight into the cause of genetic structure within the Oregon Cascades. Although the large gap in predicted-presence habitat separating Mount Hood from the Three Sisters region corresponded to a break in the distribution of mtDNA haplotypes, we observed no significant subdivision based on autosomal microsatellites or Y chromosomes. One possible explanation for this apparent contradiction is that the Maxent model performed inadequately for predicting male dispersal habitat. Alternatively, it is possible that Mount Hood and the Three Sisters region were connected indirectly by gene flow to the same population to the east (e.g., in eastern Oregon). A third possibility is that genetic effective population sizes on Mount Hood and the Three Sisters region had been larger for a longer period of time, thereby slowing their divergence from one another after isolation relative to that with the apparently smaller southern population.

Population assignments were bimodal ($q > 0.95$ for >80% of individuals) and only a few individuals exhibited admixed profiles (i.e., intermediate q), suggesting that gene flow between the two within-Cascades populations was relatively recent. The 3 admixed individuals were located mid-mountain range, consistent with a limited contact zone between the two populations. In combination with their maternal A-19a haplotypes, their genotypes suggested they were first-generation offspring with mothers from the southern population and, by inference, fathers from the northern population. Because two were females and the only male failed to produce a usable Y chromosome genotype, we had no Y chromosome confirmation of their paternal ancestry. Additionally, at least one instance of long-distance dispersal was documented, specifically, a female (OR07) that strongly assigned to the northern group but which was sampled in Crater Lake National Park. Ultimately, the small sample of individuals used to detect this subdivision necessitates genetic analysis of additional individuals from the putative contact zone and throughout the ranges to help resolve the extent and degree of admixture between the two populations.

Genetic diversity within Oregon Cascades populations — The genetic diversity of the northern population was unexpectedly high ($H_e = 0.71$), consistent with a large population that has retained much

of its ancestral diversity. However, the estimate of N_e for the northern population, although larger than for the southern population, was nevertheless relatively small, suggesting that the population could have undergone a demographic decline too recently to be reflected in the heterozygosity. Alternatively, the high heterozygosity could reflect admixture between previously distinct populations.

In contrast, the genetic diversity of the southern population was very low (He = 0.44), consistent with a small, historically isolated population. This heterozygosity was similar to contemporary California populations (Lassen He = 0.47; Sonora Pass pre-hybridization He = 0.43; Quinn et al. 2014). For this and the California populations, heterozygosities were approximately two-thirds the magnitude of the corresponding historical estimates (Lassen and Oregon combined, He = 0.70; Sierra Nevada He = 0.64), and lower than contemporary populations of other montane populations (Washington Cascades = 0.60 [Akins 2016], Idaho Rocky Mountains = 0.73 [Alden 2016]). The significantly higher average observed (average Ho = 0.51) than expected (under Hardy Weinberg equilibrium) heterozygosity in the southern Oregon population resulted in a negative F_{IS}, which, although uncommon in natural populations, is theoretically expected in very small populations (Robertson 1965, Balloux and Williams 2004, Waples 2015). The underlying principle is that large differences in allele frequencies between males and females can arise due to chance when the number of breeding adults is very small, (i.e. binomial sampling error) so that the sexes effectively represent different genetic subpopulations and their offspring appear "outbred."

Direct estimates of the genetic effective size (N_e) for the southern population based on decay of linkage disequilibrium (LD) similarly indicated a very small N_e, although several caveats render this estimate tentative. Foxes have strong pair bonds, but also have been observed to exhibit a degree of polygyny in some circumstances (e.g., Zabel and Taggart 1989), so best estimates likely fall somewhere within the range estimated under the assumption of monogamy (14.3, 95% CI = 10.5–20.4) and random mating (6.0, 3.3–9.3). More importantly, our estimates were based on only 9 individuals, which was considerably fewer than the recommended minimum sample size of 25 individuals, although the small sample size of individuals was offset to some extent by our use of a relatively large number of loci (n = 31) relative to the recommended number (10–20; Luikart et al. 2010, Tallmon et al. 2010). Small sample sizes also tend to be most problematic for populations with large N_e (i.e. low sample size to N_e ratio) (Waples and Do 2010). The most relevant concern over sample size was violation of the assumption of random sampling. Oversampling of close relatives would be expected to result in an underestimation of N_e. The LD estimator also assumed no migration, which was strictly violated (although gene flow appeared low), and would be expected to downwardly bias estimates.

Connectivity to other populations — Initially, we sought specifically to assess connectivity of the Oregon portion of the Sierra Nevada red fox subspecies to other extant populations of the Sierra Nevada red fox, particularly, the one immediately to the south on and around Lassen Peak in California, as this question was of most obvious relevance to identification of management units (e.g., Distinct Population Segment designation by the USFWS). However, our discovery in this study that the red foxes of the Oregon Cascades composed two distinct populations necessitated the broadening this comparison to other adjacent populations, in particular, to Rocky Mountain populations to the east that are presumed to be primarily native but with some with some nonnative introgression (Statham et al. 2012b, Green et al., in press). Additionally, for thoroughness, we included a comparison to the Cascade red fox of Washington, directly north across the Columbia River, although its distinctiveness had been previously demonstrated (Sacks et al. 2010). As expected, the Washington Cascade red fox was completely distinct from both Oregon populations based both on Structure and PCA analyses. Thus, below we consider the connectivity of the southern Oregon Cascade population to the Lassen population, as was our initial objective, and potential connectivity of the northern Oregon Cascade population to Rocky Mountain red fox as well as

potentially to nonnative red foxes.

The southern population was genetically distinct from all neighboring montane populations, based on both Structure and PCA analyses. In general, genetic distinctiveness of populations is a function of time since isolation and population size. Small populations become more rapidly differentiated due to genetic drift. Based on the estimated N_e of southern Oregon and Lassen populations, it seems likely that their high differentiation is at least partly due to population decline and isolation within the past century. As anticipated, we saw no evidence for contemporary gene flow between the two populations. The estimated F_{ST}, a common measure of genetic distance, also was high between southern Oregon and Lassen, similar to that observed between the two California SNRF populations (Quinn and Sacks 2014).

In contrast to the southern Oregon Cascades population, the northern population was not distinct from all neighboring populations. In particular, both Structure and PCA analyses showed the northern population to be most closely related to the Rocky Mountain (*V. v. macroura*) subspecies. The inability of either method to distinguish northern Oregon samples from the larger pool of Rocky Mountain red foxes suggests either past or recent connectivity with the *macroura* subspecies, with the most likely conduit being through the Blue Mountain ecoregion in the northeast portion of the state where *macroura* historically occurred. Since the 1990s sightings of red fox in eastern Oregon have expanded to encompass 8 counties, including unprecedented areas of open farmland as well as mountainous, historical habitat (Green et al., in press).

Lastly, the finding of nonnative haplotypes (G-38) in the Mount Hood population warrants additional concern. The likely immediate source of this introgression was the adjacent low-elevation habitats of the Columbia River Gorge and Interstate Highway 84 (I-84) corridor, as suggested by the recovery of a road-killed individual from I-84 in Hood River, <50 km to the north of the montane population that also carried the G-38 haplotype. However, it is unclear from our data whether nearby low-elevation foxes carrying G-38 haplotypes are truly nonnative or whether they are expanding Rocky Mountain red foxes that reflect a small amount of nonnative introgression. For example, the northeastern Oregon red foxes carry primarily native Rocky Mountain red fox haplotypes, but a small proportion (10%) of them carry the nonnative mitochondrial haplotype, G-38 (Green et al., in press). Preliminary microsatellite analyses of these samples indicate that the eastern Oregon foxes reflect varying degrees of nonnative admixture but no evidence of pure nonnative red foxes (C. B. Quinn, B.N. Sacks, unpublished data). Based both on mtDNA and on preliminary microsatellite analyses of the northeastern Oregon samples used by Green et al. (in press), the Columbia Plateau, potentially linked to Mount Hood via the I-84 corridor, appears to have greater prevalence of nonnative ancestry.

Given the paucity of samples in the present study from eastern Oregon and closer to the east-side of the Cascades, along I-84 and to the south, contemporary versus historical connectivity between northern Oregon Cascade and Rocky Mountain red fox populations remains somewhat unclear, as does the magnitude and significance of the nonnative red fox introgression. Addressing these questions seems a priority also for clarifying the subspecific level systematics of montane red foxes as well as the genetic integrity of native populations regardless of systematics. Regardless of connectivity of the northern Cascades population to neighboring populations, the southern Oregon population appears to reflect a very small relictual native population completely isolated from the California SNRF.

Conclusions and conservation implications

The low diversity and small N_e (uncertainty notwithstanding) together raise immediate concern regarding the long-term persistence of SNRF in Oregon. These results suggest the southern Oregon population, like those in California, has suffered a severe decline since historical times. These estimates are important for

conservation planning. First, N_e directly measures the influence of drift on a population, and is inversely related to the efficacy of selection to purge deleterious alleles or to fuel adaptation to changing climatic and environmental conditions. The southern Oregon population appears to possess similar amounts of genetic diversity to the Sonora Pass population, which has exhibited signs of inbreeding depression and reproductive deficiencies among natives (Quinn and Sacks 2014). Secondly, although ratios of effective to census population sizes vary widely, N_e serves as a loose indicator of the number of breeding adults in the population. When we factor in the large space-use requirements of montane red fox shown in other studies (Perrine 2005, Quinn and Sacks 2014; Akins 2016), it seems likely that the population is numerically small as well as genetically homogenous. Furthermore, the population occupies a smaller geographic region (i.e., south of U.S. Route 20) than we presumed prior to genetic analyses (the entire length of the Oregon Cascades).

Recommendations

1) Prioritize conservation of SNRF in the southern portion of the Cascades. Red fox in this region appear to be most vulnerable and to represent the most pristine remnant of SNRF ancestry of the Oregon Cascades.
2) Use Maxent distribution models to guide surveys within the Cascade Range with emphases on (a) gaps in detections (e.g. north and south of Willamette Pass, north of the Three Sisters), and (b) the apparent contact zone immediately north of U.S. Route 20. Additional samples are necessary to refine our understanding of substructure, effective population size, and genetic diversity.
3) Work with collaborators to obtain contemporary samples from other parts of Oregon, namely the Blue Mountain ecoregion and areas of human development immediately west and north of the Cascades. These Oregon samples can be used to compare to northern Cascade samples in admixture and population assignment analyses for more direct comparison. Reference samples of fur-farm founded populations and endemic Rocky Mountains within Oregon are necessary to resolve the origins of individuals in the northern Cascades.
4) Assess home range size, age-specific survival, density, and other demographic characteristics of SNRF through telemetry and intensive ecological study to assess capacity to serve as donor or need to serve as recipient for captive rearing and/or translocations. We acknowledge the current small-scale telemetry study near Bend, but project expansion is necessary to more fully address this recommendation.
5) Intensive sampling to estimate abundance of foxes, particularly in the southern population.

Literature Cited

Akins, J.R. 2016. Distribution, Genetic Structure, and Conservation Status of the Cascade Red Fox in Southern Washington. Doctoral dissertation. University of California, Davis.

Alden, P. B. 2016. Distribution and Origins of Red Foxes in the Great Basin. Master's Thesis. University of California, Davis.

Altschul, S. F., W. Gish, W. Miller, E. W. Myers, and D. J. Lipman. 1990. Basic local alignment search tool. Journal of molecular biology 215:403-410.

Anderson, R. P. and I. Gonzalez. 2011. Species-specific tuning increases robustness to sampling bias in models of species distributions: an implementation with Maxent. Ecological Modelling 222:2796-2811.

Aubry K.B. 1983. The Cascade red fox: distribution, morphology, zoogeoraphy and ecology. Doctoral dissertation. Seattle: University of Washington.

Aubry, K. B., M. J. Statham, B. N. Sacks, J. D. Perrine, and S. M. Wisely. 2009. Phylogeography of the North American red fox: vicariance in Pleistocene forest refugia. Molecular Ecology 18:2668-2686.

Bailey V. 1936. The mammals and life zones of Oregon. North American Fauna No. 55. Washington, D.C.: US Department of Agriculture, Bureau of Biological Survey.

Balcom, A. B. 1916. Fox farming in Prince Edward Island: a chapter in the history of speculation. The Quarterly Journal of Economics 30:665-681.

Balloux, F. and R. Williams. 2004. Heterozygote excess in small populations and the heterozygote-excess effective population size. Evolution 58:1891-1900.

Bean, W. T., R. Stafford, and J. S. Brashares. 2012. The effects of small sample size and sample bias on threshold selection and accuracy assessment of species distribution models. Ecography 35:250-258.

Boria, R. A., L. E. Olson, S. M. Goodman, and R. P. Anderson. 2014. Spatial filtering to reduce sampling bias can improve the performance of ecological niche models. Ecological Modelling 275:73-77.

Daly, C., R. P. Neilson, and D. L. Phillips. 1994. A statistical-topographic model for mapping climatological precipitation over mountainous terrain. Journal of Applied Meteorology 33:140-158.

Dormann, C. F., J. Elith, S. Bacher, C. Buchmann, G. Carl, G. Carré, J. R. G. Marquéz, B. Gruber, B. Lafourcade, and P. J. Leitão. 2013. Collinearity: a review of methods to deal with it and a simulation study evaluating their performance. Ecography 36:27-46.

Earl, D. A. 2012. STRUCTURE HARVESTER: a website and program for visualizing STRUCTURE output and implementing the Evanno method. Conservation Genetics Resources 4:359-361.

Elith, J., S. J. Phillips, T. Hastie, M. Dudík, Y. E. Chee, and C. J. Yates. 2011. A statistical explanation of MaxEnt for ecologists. Diversity and Distributions 17:43-57.

Engler, R., A. Guisan, and L. Rechsteiner. 2004. An improved approach for predicting the distribution of rare and endangered species from occurrence and pseudo□absence data. Journal of Applied Ecology 41:263-274.

Evanno, G., S. Regnaut, and J. Goudet. 2005. Detecting the number of clusters of individuals using the software STRUCTURE: a simulation study. Molecular Ecology 14:2611-2620.

Falush, D., M. Stephens, and J. K. Pritchard. 2003. Inference of population structure using multilocus genotype data: linked loci and correlated allele frequencies. Genetics 164:1567-1587.

Galpern, P., M. Manseau, P. Hettinga, K. Smith, and P. Wilson. 2012. Allelematch: an R package for identifying unique multilocus genotypes where genotyping error and missing data may be present. Molecular Ecology Resources 12:771-778.

Goudet, J. 2001. FSTAT, a program to estimate and test gene diversities and fixation indices (version 2.9. 3).

Green, G. A., B. N. Sacks, L. J. Erickson, and K. B. Aubry. in press. Genetic Characteristics of Red Fox in Northeastern Oregon. Northwestern Naturalist.

Grinnell J, Dixon JS, Linsdale JM. 1937. Fur-bearing mammals of California. Volume II, Berkeley, California: University of California Press.

Guisan, A., O. Broennimann, R. Engler, M. Vust, N. G. Yoccoz, A. Lehmann, and N. E. Zimmermann. 2006. Using niche□based models to improve the sampling of rare species. Conservation Biology 20:501-511.

Hernandez, P. A., C. H. Graham, L. L. Master, and D. L. Albert. 2006. The effect of sample size and species characteristics on performance of different species distribution modeling methods. Ecography 29:773-785.

Hijmans, R. J. 2012. Cross□validation of species distribution models: removing spatial sorting bias and calibration with a null model. Ecology 93:679-688.

Hijmans, R. J. 2016. raster: Geographic data analysis and modeling. R package version 2.5-8. https://CRAN.R-project.org/package=raster.

Hijmans, R. J., S. E. Cameron, J. L. Parra, P. G. Jones, and A. Jarvis. 2005. Very high resolution interpolated climate surfaces for global land areas. International Journal of Climatology 25:1965-1978.

Hiller, T. L., J. E. McFadden-Hiller, and B. N. Sacks. 2015. Genetic and Photographic Detections Document Sierra Nevada Red Fox in the Northern Cascades of Oregon. Northwest Science 89:409–413.

Ingles LG. 1965. Mammals of the Pacific states: California, Oregon, and Washington. Stanford, California: Stanford University Press.

Jombart, T. 2008. adegenet: a R package for the multivariate analysis of genetic markers. Bioinformatics 24:1403-1405.

Kalinowski, S. T., M. L. Taper, and T. C. Marshall. 2007. Revising how the computer program CERVUS accommodates genotyping error increases success in paternity assignment. Molecular Ecology 16:1099-1106.

Kalle, R., T. Ramesh, Q. Qureshi, and K. Sankar. 2013. Predicting the Distribution Pattern of Small Carnivores in Response to Environmental Factors in the Western Ghats. PloS One 8:e79295.

Kasprowicz, A. E., M. J. Statham, and B. N. Sacks. 2016. Fate of the other redcoat: remnants of colonial British foxes in the Eastern United States. Journal of Mammalogy 97:298-309.

Kramer□Schadt, S., J. Niedballa, J. D. Pilgrim, B. Schröder, J. Lindenborn, V. Reinfelder, M. Stillfried, I. Heckmann, A. K. Scharf, and D. M. Augeri. 2013. The importance of correcting for sampling bias in MaxEnt species distribution models. Diversity and Distributions 19:1366-1379.

Laut, A. C. 1921. The fur trade of America. New York: Macmillan.

Lobo, J. M., A. Jiménez□Valverde, and R. Real. 2008. AUC: a misleading measure of the performance of predictive distribution models. Global ecology and Biogeography 17:145-151.

Loiselle, B. A., C. A. Howell, C. H. Graham, J. M. Goerck, T. Brooks, K. G. Smith, and P. H. Williams. 2003. Avoiding pitfalls of using species distribution models in conservation planning. Conservation biology 17:1591-1600.

Luikart, G., N. Ryman, D. A. Tallmon, M. K. Schwartz, and F. W. Allendorf. 2010. Estimation of census and effective population sizes: the increasing usefulness of DNA-based approaches. Conservation Genetics 11:355-373.

McCune, B., D. Keon, and R. Marrs. 2002. Equations for potential annual direct incident radiation and heat load. Journal of Vegetation Science 13:603-606.

Merow, C., M. J. Smith, and J. A. Silander. 2013. A practical guide to MaxEnt for modeling species' distributions: what it does, and why inputs and settings matter. Ecography 36:1058-1069.

Merson, C., M. J. Statham, J. E. Janecka, R. R. Lopez, N. J. Silvy, and B. N. Sacks. 2017. Distribution of native and nonnative ancestry in red foxes along an elevational gradient in central Colorado. Journal of Mammalogy 98:365-377.

Moore, M., S. Brown, and B. Sacks. 2010. Thirty-one short red fox (Vulpes vulpes) microsatellite markers. Molecular Ecology Resources 10:404-408.

Muscarella, R., P. J. Galante, M. Soley□Guardia, R. A. Boria, J. M. Kass, M. Uriarte, and R. P. Anderson. 2014. ENMeval: an R package for conducting spatially independent evaluations and estimating optimal model complexity for Maxent ecological niche models. Methods in Ecology and Evolution 5:1198-1205.

Naimi, B. 2015. usdm: Uncertainty Analysis for Species Distribution Models. R package version 1.1-15. https://CRAN.R-project.org/package=usdm.

Neale, J. C. and B. N. Sacks. 2001. Resource utilization and interspecific relations of sympatric bobcats and coyotes. Oikos 94:236-249.

Park, S. 2001. The Excel microsatellite toolkit. Trypanotolerance in West African Cattle and the Population Genetic Effects of Selection.

Perrine, J. D. 2005. Ecology of red fox (Vulpes vulpes) in the Lassen Peak region of California, USA. University of California, Berkeley.

Perrine, J. D., J. P. Pollinger, B. N. Sacks, R. H. Barrett, and R. K. Wayne. 2007. Genetic evidence for the persistence of the critically endangered Sierra Nevada red fox in California. Conservation Genetics 8:1083-1095.

Peterson, A. T., M. Papeş, and J. Soberón. 2008. Rethinking receiver operating characteristic analysis applications in ecological niche modeling. Ecological Modelling 213:63-72.

Phillips, S. J., R. P. Anderson, and R. E. Schapire. 2006. Maximum entropy modeling of species geographic distributions. Ecological Modelling 190:231-259.

Phillips, S. J. and M. Dudík. 2008. Modeling of species distributions with Maxent: new extensions and a comprehensive evaluation. Ecography 31:161-175.

Preckler-Quisquater, S., K. Miles, T. Batter, S. Anderson, and B. N. Sacks. 2017. Occupancy estimation as a tool to test and refine a predictive species distribution model for the Sacramento Valley red fox (Vulpes vulpes patwin). The Wildlife Society Western Section, Reno.

Pritchard, J. K., M. Stephens, and P. Donnelly. 2000. Inference of population structure using multilocus genotype data. Genetics 155:945-959.

Quinn CB, Sacks BN. 2014. Ecology, distribution, and genetics of Sierra Nevada Red Fox. Report to California Department of Fish and Wildlife.

Radosavljevic, A. and R. P. Anderson. 2014. Making better Maxent models of species distributions: complexity, overfitting and evaluation. Journal of Biogeography 41:629-643.

Rando et al., in review. Y chromosome microsatellites for the red fox.

Rice, W. R. 1989. Analyzing Tables of statistical tests. Evolution 43:223-225.

Robertson, A. 1965. The interpretation of genotypic ratios in domestic animal populations. Animal Production 7:319-324.

Sacks, B. N., J. L. Brazeal, and J. C. Lewis. 2016. Landscape genetics of the nonnative red fox of California. Ecology and Evolution 6:4775-4791.

Sacks BN, Quinn CB, Alden PB. 2015. Sierra Nevada Red Fox Monitoring: Phase I. Report to US Forest Service Region 5.

Sacks, B. N., H. U. Wittmer, and M. J. Statham. 2010. The native Sacramento Valley red fox. Report to the California Department of Fish and Game.

Shcheglovitova, M. and R. P. Anderson. 2013. Estimating optimal complexity for ecological niche models: a jackknife approach for species with small sample sizes. Ecological Modelling 269:9-17.

Statham, M. J., J. Murdoch, J. Janecka, K. B. Aubry, C. J. Edwards, C. D. Soulsbury, O. Berry, Z. Wang, D. Harrison, and M. Pearch. 2014. Range□wide multilocus phylogeography of the red fox reveals ancient continental divergence, minimal genomic exchange and distinct demographic histories. Molecular Ecology 23:4813-4830.

Statham, M. J., A. C. Rich, S. K. Lisius, and B. N. Sacks. 2012a. Discovery of a remnant population of Sierra Nevada red fox (Vulpes vulpes necator). Northwest Science 86:122-132.

Statham, M. J., B. N. Sacks, K. B. Aubry, J. D. Perrine, and S. M. Wisely. 2012b. The origin of recently established red fox populations in the United States: translocations or natural range expansions? Journal of Mammalogy 93:52-65.

Tallmon, D. A., D. Gregovich, R. S. Waples, C. Scott Baker, J. Jackson, B. L. Taylor, E. Archer, K. K. Martien, F. W. Allendorf, and M. K. Schwartz. 2010. When are genetic methods useful for

estimating contemporary abundance and detecting population trends? Molecular Ecology Resources 10:684-692.

Toonen, R. J. and S. Hughes. 2001. Increased throughput for fragment analysis on an ABI Prism® 377 automated sequencer using a membrane comb and STRand software. Biotechniques 31:1320-1325.

U.S. Fish and Wildlife Service. 2015a. SPECIES REPORT: Sierra Nevada Red Fox (*Vulpes vulpes necator*). August 14, 2015. https://www.fws.gov/sacramento/ outreach/2015/10-07/docs/20150814_SNRF_SpeciesReport.pdf

U.S. Fish and Wildlife Service. 2015b. Endangered and Threatened Wildlife and Plants; 12-Month Finding on a Petition To List Sierra Nevada Red Fox as an Endangered or Threatened Species; Proposed Rule. Federal Register 50: 60990-61028

Verts, B. and L. N. Carraway. 1998. Land mammals of Oregon. Berkeley, California: Univ of California Press.

Volkmann, L. A., M. J. Statham, A. Ø. Mooers, and B. N. Sacks. 2015. Genetic distinctiveness of red foxes in the Intermountain West as revealed through expanded mitochondrial sequencing. Journal of Mammalogy 96:297-307.

Wandeler, P. and S. Funk. 2006. Short microsatellite DNA markers for the red fox (Vulpes vulpes). Molecular Ecology Notes 6:98-100.

Waples, R. S. 2006. A bias correction for estimates of effective population size based on linkage disequilibrium at unlinked gene loci. Conservation Genetics 7:167-184.

Waples, R. S. 2015. Testing for Hardy–Weinberg proportions: have we lost the plot? Journal of Heredity 106:1-19.

Waples, R. S. and C. Do. 2008. LDNE: a program for estimating effective population size from data on linkage disequilibrium. Molecular Ecology Resources 8:753-756.

Waples, R. S. and C. Do. 2010. Linkage disequilibrium estimates of contemporary Ne using highly variable genetic markers: a largely untapped resource for applied conservation and evolution. Evolutionary Applications 3:244-262.

Warren D.L. and Seifert S.N. 2011. Ecological niche modeling in Maxent: the importance of model complexity and the performance of model selection criteria. Ecological Applications 21:335-342.

Wisz, M. S., R. Hijmans, J. Li, A. T. Peterson, C. Graham, and A. Guisan. 2008. Effects of sample size on the performance of species distribution models. Diversity and distributions 14:763-773.Yackulic, C. B., R. Chandler, E. F. Zipkin, J. A. Royle, J. D. Nichols, E. H. Campbell Grant, and S. Veran. 2013. Presence□only modelling using MAXENT: when can we trust the inferences? Methods in Ecology and Evolution 4:236-243.

Zabel C.J. and Taggart S.J. 1989. Shift in red fox, Vulpes vulpes, mating system associated with El Niño in the Bering Sea. Animal Behaviour **38**:830-838.

Table 1. Results of genetic analysis for 78 red fox DNA samples collected between 2010–2016, Oregon, USA, including samples in the Oregon Cascade Range (n = 73), and nearby regions (Mount Hood n = 1; Deschutes County n = 4; Malheur County n = 1).

Lab ID	Field ID	Sample Type	Lat	Lon	Date Collected	Genetic Sex	mtDNA Haplo	Indiv ID
S12-1157	20120808-1	hair	42.8903	-122.08161	8/8/2012		A-19	
S12-1158	20120808-2	hair	42.8903	-122.08161	8/8/2012		A-19	
S12-1225*	20120918	hair	45.7055	-121.59046	9/18/2012	M	G-?	OR01
S13-0512	FS08	scat	44.4586	-121.84847	1/4/2013		A-19	
S13-0513	FS10	scat	44.4585	-121.83586	1/4/2013	F	A-19	OR02
S13-0514	FS10B	scat	44.4585	-121.83586	1/4/2013		A-19	OR02
S13-0515	W57	scat	44.4554	-121.8476	1/4/2013		A-19	OR02
S13-1198	F5a,b,c	hair	44.2693	-121.78003	4/23/2013	F	A-19	OR03
S13-1356	20110511jaS01	scat	45.3272	-121.67121	5/11/2011	M	G-38	OR04
S13-1624	20130512PSS01	scat	45.3397	-121.63381	5/12/2013	M	A-19	OR05
S13-1625	20130330TLS01	scat	45.3295	-121.70645	3/30/2013	F	G-38	OR06
S13-1628	20121104PSS01	scat	45.3422	-121.74023	11/4/2012	M	G-38	
S13-2080	CRLA-01	scat	42.9214	-122.02947	6/24/2013	F	A-19	OR07
S13-2278	CRLA-02	scat	42.9291	-122.03266	7/8/2013		A-19	OR07
S13-2559	CRLA-02	tissue	42.8699	-122.1442	7/27/2013	F	A-19	OR08
S14-0333	FS06	scat	44.455	-121.84711	12/13/2013	F	A-19	OR02
S14-0334	W48	scat	43.9938	-121.65555	12/17/2013		A-?	
S14-0346	HD01	scat	44.395	-121.88682	1/14/2014		A-?	
S14-0827	WPN-1 to WPN-8	hair	43.6164	-122.04028	4/29/2014		A-?	
S14-1006	sample 1	hair	44.3968	-121.88907	6/19/2014		A-19	
S14-1007	sample 2	hair	44.3968	-121.88907	6/19/2014		A-19	
S14-1052	FS01	scat	44.4025	-121.87333	5/2/2014		A	
S14-1053	FS02	scat	44.4036	-121.87222	5/2/2014		A	
S14-1054	FS02	scat	44.4022	-121.87502	6/9/2014	F	A-?	OR10
S14-1260	20140714-2	scat	44.0174	-121.44085	7/14/2014		A-19	
S14-1262	20140714-1	scat	44.0174	-121.43511	7/14/2014		A	
S14-1264	20140714-2	scat	44.02	-121.44	7/14/2014		A	
S14-1266	20140714	scat	44.02	-121.44	7/14/2014		A-19	
S14-1343	WP-01	scat	43.6031	-122.0386	7/15/2014	F	A	OR11
S14-1344	WP-02	scat	43.6031	-122.0386	7/15/2014		A-19	
S14-2259	20140902-2	scat	43.5945	-122.01089	9/2/2014	F	A	OR11
S14-2260	20140902-3	scat	43.5942	-122.01018	9/2/2014	F	A	OR11
S14-2262	20140902-1	scat	43.5968	-122.02079	9/2/2014	F	A-19	
S14-2263	20140902-2	scat	43.5972	-122.02911	9/2/2014	F	A-19	
S14-2265	20140903-2	scat	43.5965	-121.9997	9/3/2014		A-19	
S14-2266	20140903-3	scat	43.5946	-122.02179	9/3/2014	F	A	OR11
S14-2268	20140903-2	scat	43.5939	-122.0084	9/3/2014		A-19	
S14-2270	20140905-4	scat	43.5904	-122.06396	9/15/2014		A-19	
S14-2271	20140915-2	scat	43.5871	-122.05305	9/15/2014	M	A	OR12
S14-2274	20140915-2	scat	43.5869	-122.05333	9/15/2014	M	A	OR12
S14-2275	20140915-3	scat	43.5903	-122.05827	9/15/2014	F	A	OR11

S14-2276	20140915-1	scat	43.582	-122.05918	9/15/2014		A-19	
S14-2279	20140915-3	scat	43.5918	-122.05408	9/15/2014	F	A-19	
S14-2280	20140915-3	scat	43.5918	-122.05682	9/15/2014	M	A	OR12
S14-2284	20140916-1	scat	43.5787	-122.06901	9/16/2014	M	A	OR12
S14-2289	20140917-3	scat	43.5745	-122.05877	9/17/2014		A	OR11
S14-2302	20140918-2	scat	43.6091	-121.9493	9/18/2014		A-19	OR13
S14-2303	20140918-3	scat	43.609	-121.94938	9/18/2014		A-19	
S14-2304	20140918-4	scat	43.6122	-121.95463	9/18/2014	M	A-19	OR14
S14-2305	20140918-1	scat	43.6081	-121.94328	9/18/2014	M	A	OR13
S14-2306	20140918-2	scat	43.609	-121.95024	9/18/2014		A-19	
S14-2307	20140918-3	scat	43.6121	-121.95232	9/18/2014		A-19	
S14-2308	20140704PHS01	scat	45.3373	-121.72708	7/4/2014		G-38	
S14-2315	20140817PHS02	scat	45.3809	-121.66135	8/17/2014		G-38	
S14-2316	20140922SAS01	scat	45.3889	-121.65963	9/22/2014		G-38	
S14-2332	20140930AHS01	scat	45.3706	-121.65866	9/30/2014	F	G-38	OR15
S14-2560	Will Pass - 1	scat	43.604	-122.041	10/13/2014	M	A-?	
S14-2561	Will Pass - 2	scat	43.611	-122.043	10/13/2014	M	A-?	OR16
S14-2563	Will Pass - 4	scat	43.61	-122.039	10/13/2014	M	A	OR12
S14-2564	Will Pass - 5	scat	43.61	-122.04	10/13/2014	M	A	OR12
S15-1040	WP-3	scat	43.6071	-122.04618	6/5/2015	M	A	OR12
S15-1041	WP-4	scat	43.6071	-122.04618	6/5/2015		A-?	
S15-1042	WP-5	scat	43.6071	-122.04618	6/5/2015		A-19	
S15-1043	WP-6	scat	43.6071	-122.04618	6/5/2015	F	A-19	OR11
S15-1044	WP-7	scat	43.6071	-122.04618	6/5/2015		A-?	
S15-1382	CRLA 17	scat	42.8957	-122.13667	7/28/2015	M	A-19	OR17
S15-1552*	20150209MG01	hair	44.1602	-121.30389	2/9/2015	M	A-19	OR18
S15-1557*	20150711HDMH01	hair	44.1677	-121.34963	7/11/2015	M	A-19	OR19
S15-1560	20150615MGS02	scat	43.9822	-121.64922	6/15/2015	F	A-?	
S15-1565*	20150711HDMS01	scat	44.1674	-121.34797	7/11/2015	M	A-19	OR19
S15-1566*	20150711HDMS02	scat	44.168	-121.34731	7/11/2015	M	A-19	OR20
S15-1950	20150806RWS01	scat	44.4412	-121.79432	8/6/2015		A-?	
S16-0024	20150713-1	scat	43.9998	-121.86544	7/13/2015	F	A-19	OR21
S16-0025	20150713-2	scat	43.9982	-121.86705	7/13/2015		A-19	
S16-1325	20141109TWS01	scat	44.0037	-121.82582	11/9/2014		A-19	
S16-4635*†		hair	43.35146	-119.01628	2016	F	A-19	OR23
S16-5474	01-07212016ARS	scat	42.9175	-122.02028	7/21/2016	M	A	OR22
S16-5492	01-08052016NCW	scat	42.8853	-122.08	8/5/2016	M	A-19	OR22

* Samples adjacent to the Cascade ecoregion that were included in genetic analyses but not used in Maxent species distribution modeling

† Sample from Malheur County that was included in genetic Structure analysis for reference, but was not assigned to a population due to its geographic distance from the Cascade ecoregion.

Table 2. Percent contribution of predictor variables for Maxent models built using confirmed (verified through digital images and genetic samples collected during 2010–2016; n = 124) and inclusive (verified and unverified data collected during 1985–2016; n = 169) datasets of red fox detections in the Oregon Cascades, with default and optimum regularization settings. Land-cover type followed by minimum January temperature had the greatest influence in all model variations.

	Confirmed		Inclusive	
	Default $\beta = 1$	Optimum $\beta = 3$	Default $\beta = 1$	Optimum $\beta = 2.5$
Land-cover	74.4	77.9	48.4	45.9
Min. Jan. Temp	8.4	12.2	26.5	31.4
Precip. Seasonality	6.4	0.0	0.1	17.6
Isothermality	4.5	1.4	0.9	1.3
Temp. Seasonality	2.8	1.3	0.5	0.9
Canopy Cover	2.3	0.0	18.1	2.0
Aspect	0.9	0.0	2.7	0.7
Roughness	0.3	0.0	2.8	0.1
Dec. Precip.	0.0	7.3	0.1	0.2

Table 3. Table of average AUC values estimated from spatial cross-validation of Maxent predictions for red fox in the Oregon Cascades. In both datasets, evaluation using the full or training data (AUC_{FULL}, AUC_{TRAIN}) were greatest for default models, but increased regularization improved the models' abilities to predict spatially independent test data (AUC_{TEST}) and reduced the difference between test and training performance (AUC_{DIFF}).

Input Data	Regularization (β)	AUC_{FULL}	AUC_{TRAIN}	AUC_{TEST}	AUC_{DIFF}
Confirmed	1 (default)	0.844*	0.838 (0.003)*	0.668 (0.004)	0.170 (0.005)
	3 (optimum)	0.806	0.857 (0.001)	0.784 (0.026)*	0.074 (0.032)*
Inclusive	1 (default)	0.819*	0.823 (0.001)*	0.758 (0.001)	0.065 (0.004)
	2.5 (optimum)	0.796	0.803 (0.000)	0.779 (0.005)*	0.023 (0.003)*

* better performing model for each dataset (i.e., confirmed, inclusive)

Table 4. Proportion of red fox occurrence records and proportion and area of Oregon Cascade study area encompassed by predicted presence after threshold decisions were applied to Maxent distribution models. Table demonstrates tradeoff between proportion and total area of study area predicted as presence (specificity) and proportion of occurrence records encompassed by prediction (sensitivity) depending on threshold criteria.

Input Data	Regularization (β)	Threshold Probabilities	Proportion of Presences	Proportion of Study Area	Area (km^2)
Confirmed	1 (default)	0.268	0.91	0.12	6,914
		0.499	0.73	0.04	2,439
	3 (optimum)	0.268	0.94	0.41	23,103
		0.499	0.73	0.06	3,223
Inclusive	1 (default)	0.268	0.90	0.25	13,907
		0.499	0.66	0.07	3,786
	2.5 (optimum)	0.268	0.94	0.36	20,394
		0.499	0.63	0.08	4,432

Table 5. Genetic samples collected 2010-2016, Oregon, USA.

Species	Hair	Scat	Tissue	Total
DNA failed to amplify	2	75	2	79
Coyote	--	95	--	95
Marten	4	63	--	67
Bobcat	--	47	--	47
Other species*	8	15	--	23
Red Fox	10	67	1	78
Total	24	362	3	389

*Other species included black bear, striped skunk, domestic dog, marmot, flying squirrel, and black-tailed deer (from hair brushes)

Table 6. Y-haplotypes for 9 male individual red fox in the Oregon Cascades, 2010-2016, based on 15 linked microsatellite loci.

Lab ID	Indiv ID	Pop	Y Haplo	VVY 10a	VVY 10b	VVY 10c	VVY 11	VVY 13	VVY 14a	VVY 16	VV Y17	VVY 3	VVY 5a	VVY 5b	VVY 7	VVY 8a	Y29	Y30
S14-2304	OR14	South	1	304	308	312	294	402	135	201	236	414	206	210	264	106	176	387
S16-5492	OR22	South	1	304	308	312	294	402	135	201	236	414	206	210	264	106	176	387
S14-2563	OR12	South	1	304	-	312	294	-	135	201	-	-	206	210	264	106	176	-
S15-1382	OR17	South	1	304	-	-	294	-	135	201	-	414	206	210	-	106	176	-
S14-2561	OR16	South	1	-	308	-	294	-	-	-	-	-	206	210	-	106	176	387
S13-1624	OR05	North	2	304	306	312	294	402	135	201	236	-	206	212	252	106	174	387
S15-1552	OR18	North	3	-	306	312	294	402	135	201	236	414	204	216	264	106	178	387
S15-1566	OR20	North	4	304	306	316	294	-	135	199	236	394	206	208	256	106	172	387
S15-1565	OR19	North	4	304	306	316	294	402	135	199	-	394	206	-	256	106	172	387

Table 7. Genetic diversity estimated for red fox in the Oregon Cascades and Lassen, California, using 31 microsatellites, including expected heterozygosity (H_e), observed heterozygosity (H_o), average number of alleles per locus (Avg No. alleles), and genetic effective population sizes (N_e) under assumptions of monogamy and random mating. Red fox individuals were assigned to north and south populations within the Oregon Cascades according to Structure results in Fig. 7, excluding q-values <0.7.

Pop	n	H_e (SD)	H_o (SD)	F_{IS}	Avg No. alleles (SD)	AR	N_e (95% CI) Monog.	N_e (95% CI) Rand. Mating
North Oregon	10	0.71 (0.02)	0.67 (0.03)	0.065	5.0 (2.2)	4.4	47.6 (36.5–66.5)	23.0 (17.5–32.4)
South Oregon	8	0.44 (0.04)	0.51 (0.03)	-0.172*	2.9 (1.6)	3.0	14.3 (10.5–20.4)	6.0 (3.3–9.3)
Total	21	0.67 (0.02)	0.60 (0.19)	0.112*	5.6 (0.9)	4.3	18.2 (16.5–20.2)	8.2 (7.3–9.2)
Lassen	12	0.47 (0.03)	0.49 (0.03)	-0.030	2.6 (0.8)	2.0	4.2 (6.6 – 7.4)	2.1 (1.8 – 2.4)

Table 8. Pairwise F_{ST} of montane red fox populations in the western US based on 31 autosomal microsatellites.

	North Oregon	South Oregon	Lassen	Rockies	Washington
North Oregon	-				
South Oregon	0.180	-			
Lassen	0.189	0.339	-		
Rockies	0.040	0.140	0.188	-	
Washington	0.211	0.313	0.336	0.161	-
Sierra Nevada	0.251	0.396	0.369	0.212	0.446

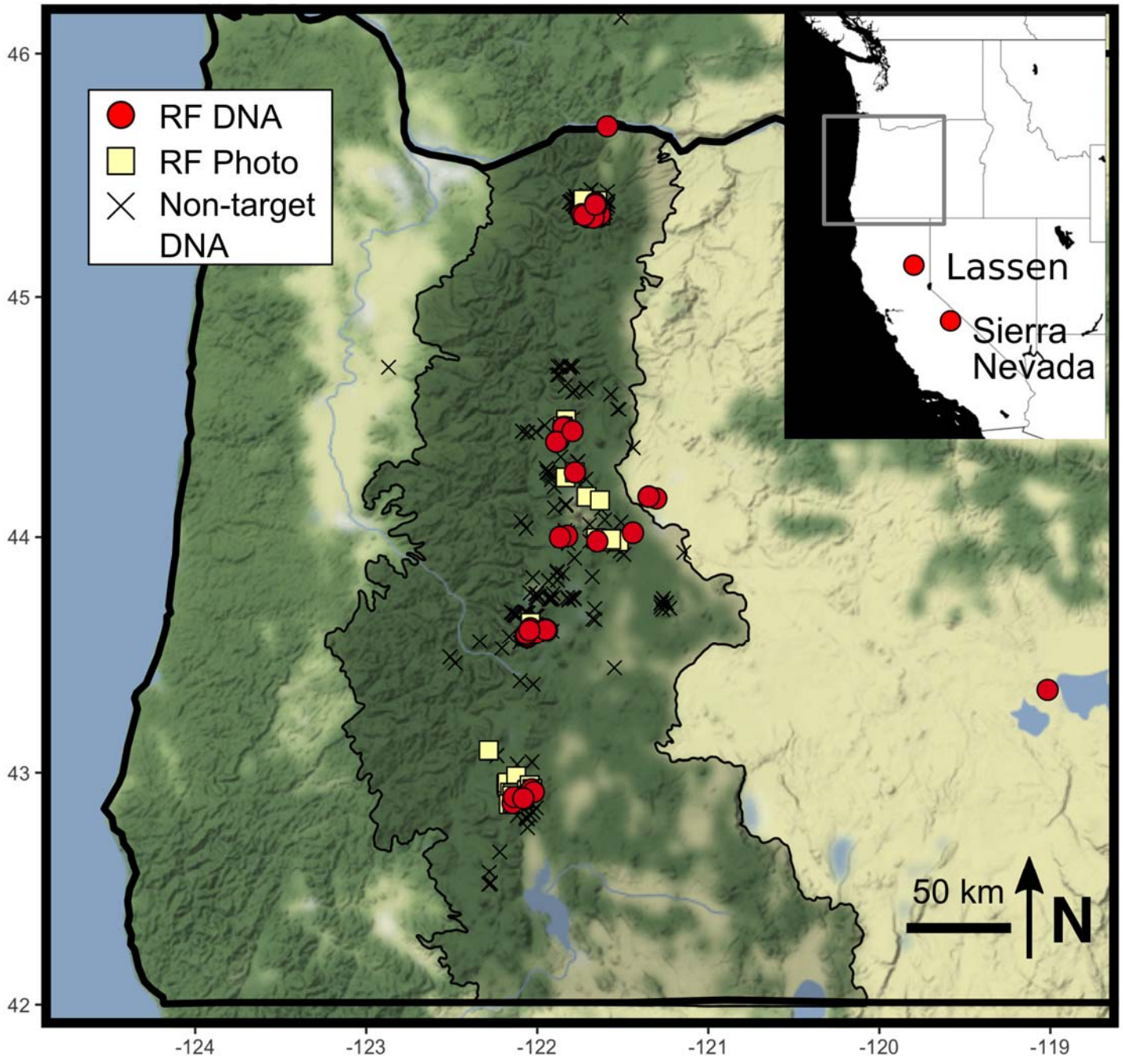

Figure 1. Locations of red fox detections 2010-2016 referenced in this report, including detections in the East and West Cascade ecoregions (genetic n = 78; photographs/digital images n = 37), and detections from neighboring regions (Hood River County n = 1; Deschutes County n = 3; Malheur County n =1), Oregon, USA. Genetic samples that failed to amplify or were identified as other species (n = 232) are shown as an index of survey intensity for genetic scat searches.

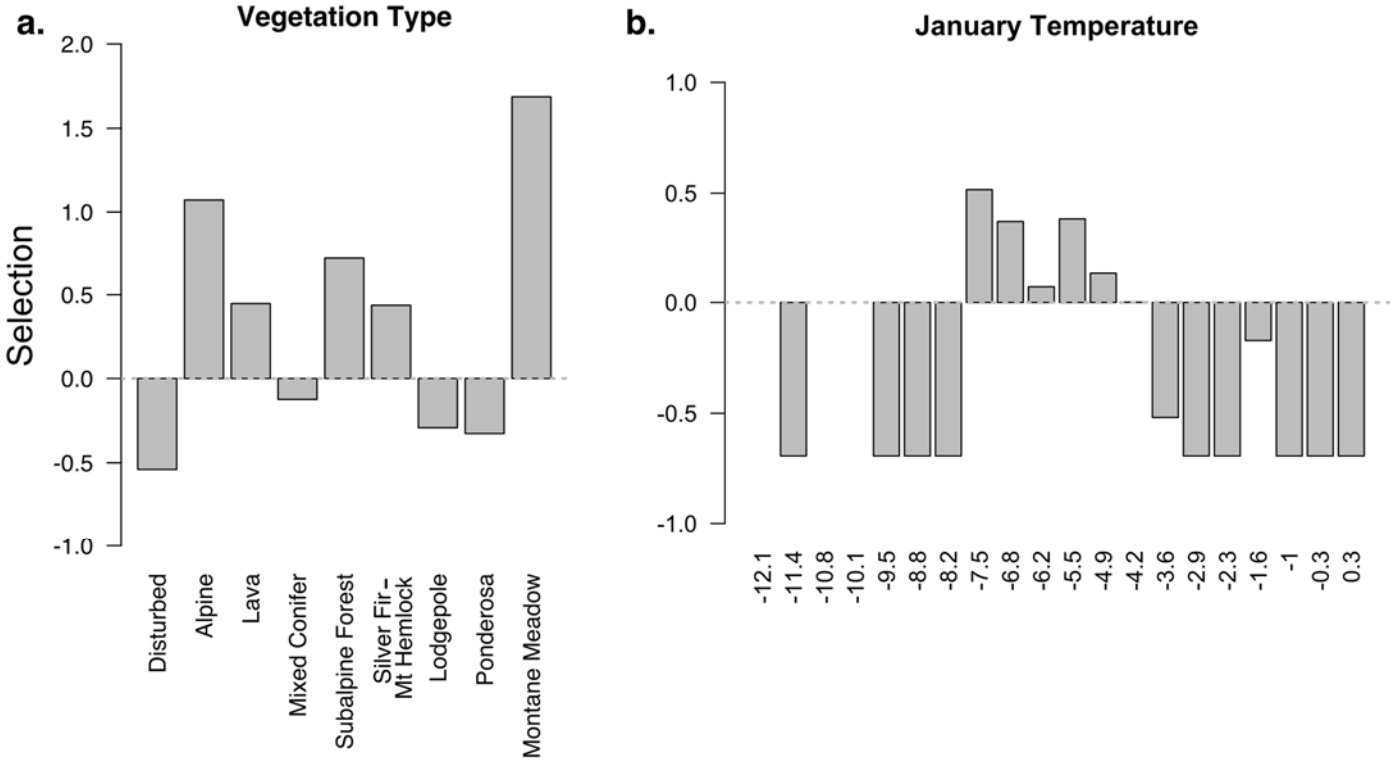

Fig 2. Indices of selection for variables with the strongest relationship, land-cover class (vegetation) and minimum January temperature. Selection was caluclated using ln(observed occurrences/expected occurrences + 1) – ln(2). Positive and negative numbers indicate use of an environmental class proportionately greater and less than expected based on the composition of the study area. (Only land-cover classes where red fox were detected are shown.)

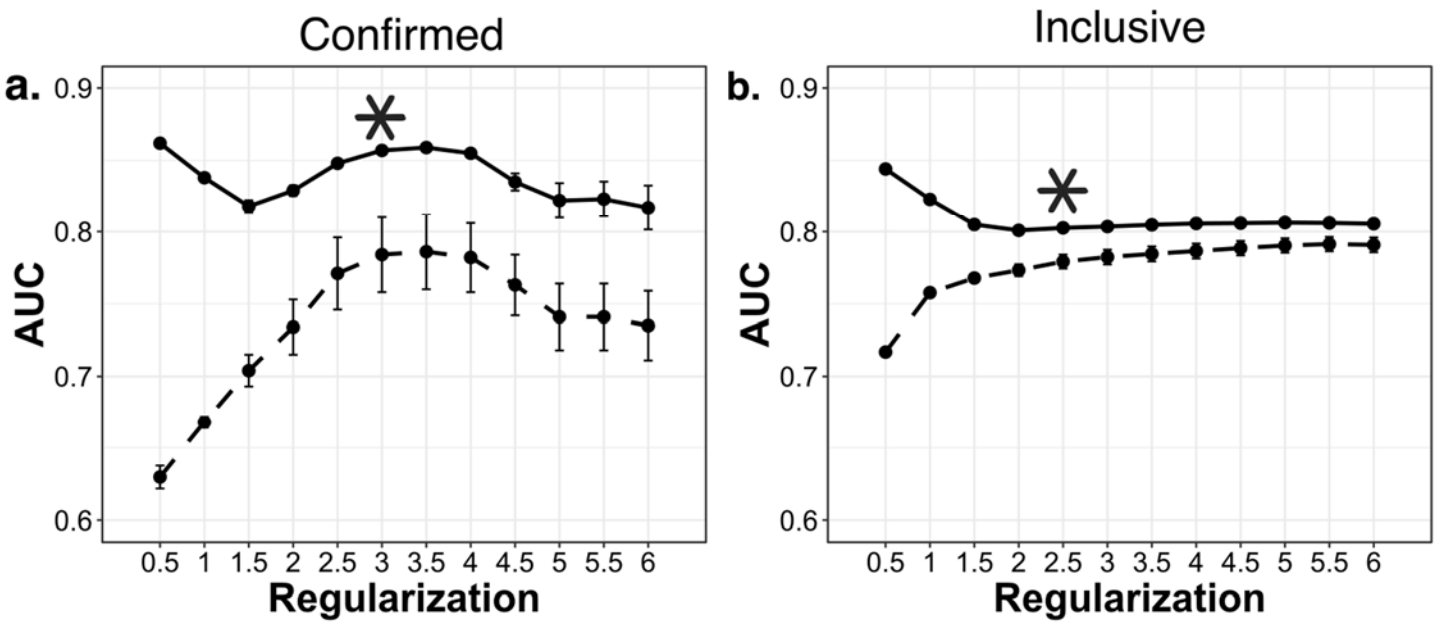

Figure 3. Average Maxent AUC values of spatially binned training (solid line) and test (dotted line) red fox occurrence data across a range of regularization values (β) for confirmed and inclusive datasets. We chose optimal values (*) where gains in AUC_{TEST} plateaued and the difference between test and training scores were minimal.

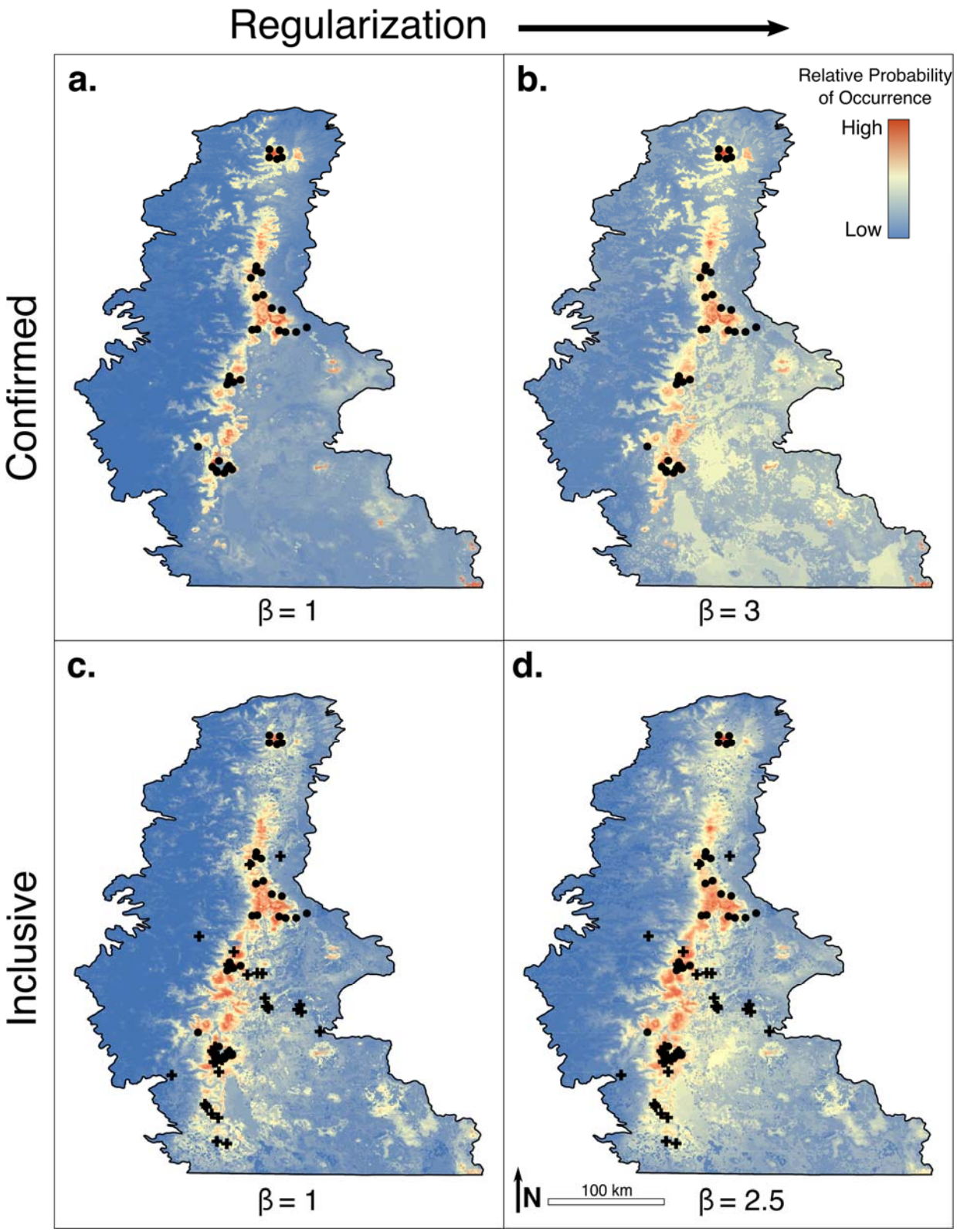

Figure 4. Logistic projections of predicted relative occurrence of red fox in the Cascade ecoregion, based on Maxent modeling of confirmed and inclusive occurrence datasets, for default and optimal regularization settings (●= confirmed occurrence, + = unverified sighting).

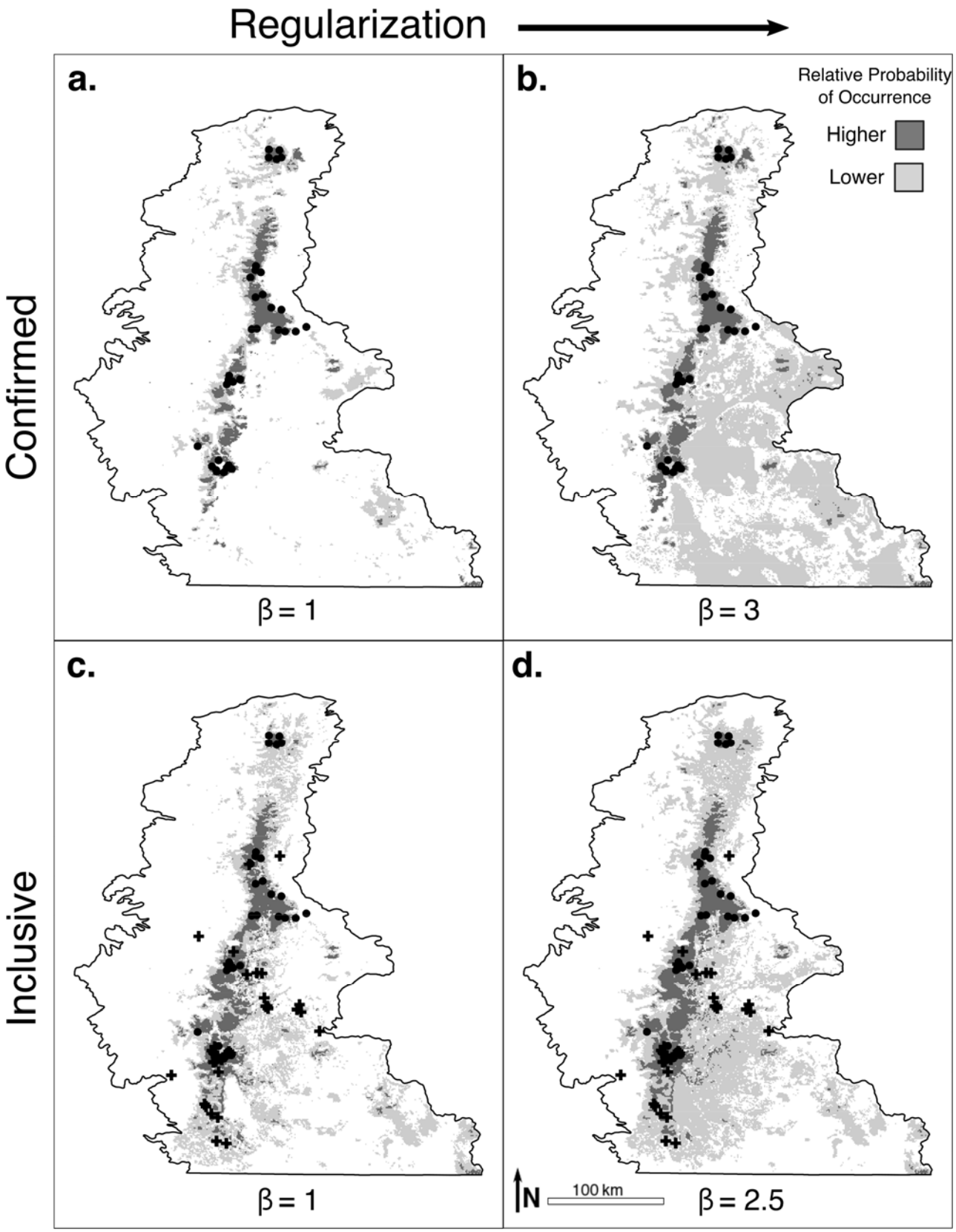

Figure 5. Dichotomized Maxent predictions showing area of predicted presence using a restrictive threshold (>0.50; dark gray) and relaxed threshold (>0.27; light gray). Thresholds were determined by maximizing the difference between estimates of sensitivity and proportion of study area included in predicted presence (●= confirmed occurrence, + = unverified sighting).

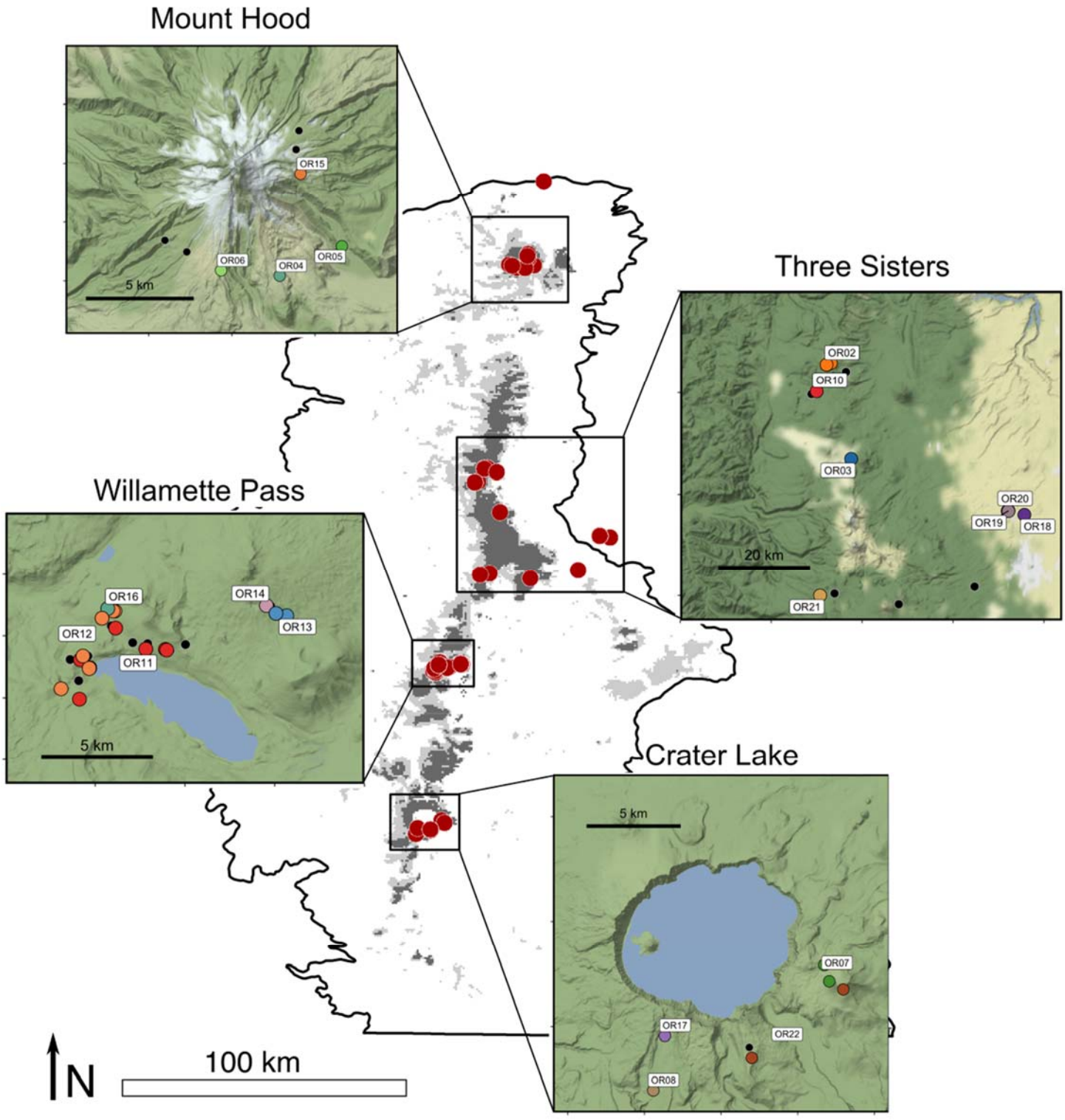

Figure 6. Distribution of red fox genetic samples identified to individual using 31 autosomal microsatellites, 2010-2016, Oregon Cascades, USA. Filled black circles represent genetic samples from red fox that failed to amplify a sufficient number of microsatellite loci for individual identification.

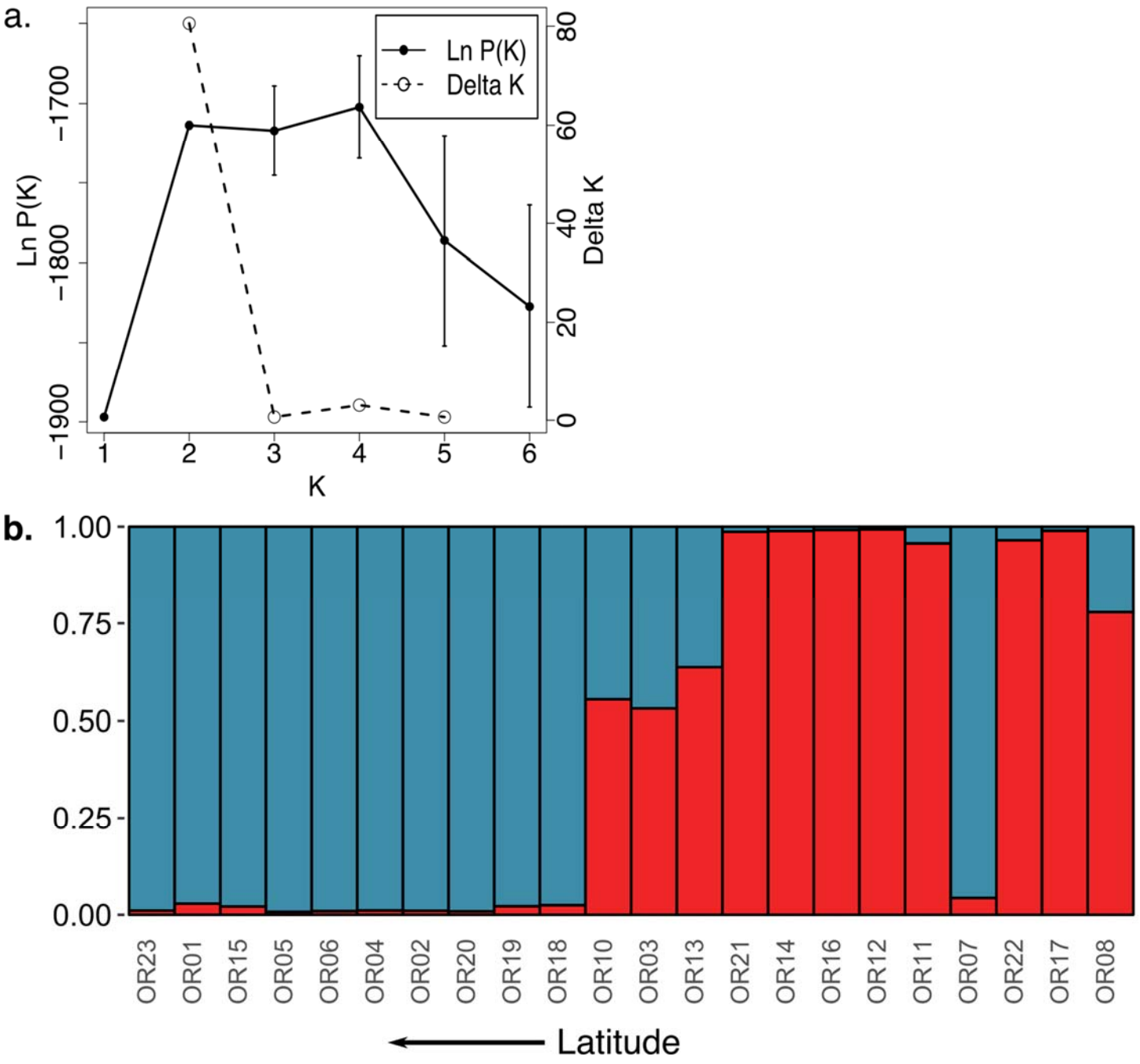

Figure 7. a) Diagnostic plot of 10 replicate Structure runs indicating greatest support for K = 2 distinct genetic clusters based on the first peak in the likelihood of the data [Ln P(K)] with low variance, and the delta K mode. b) Proportion of ancestry indicated by Structure analysis at K = 2 genetic clusters for red fox individuals in the Oregon Cascades, 2010-2016.

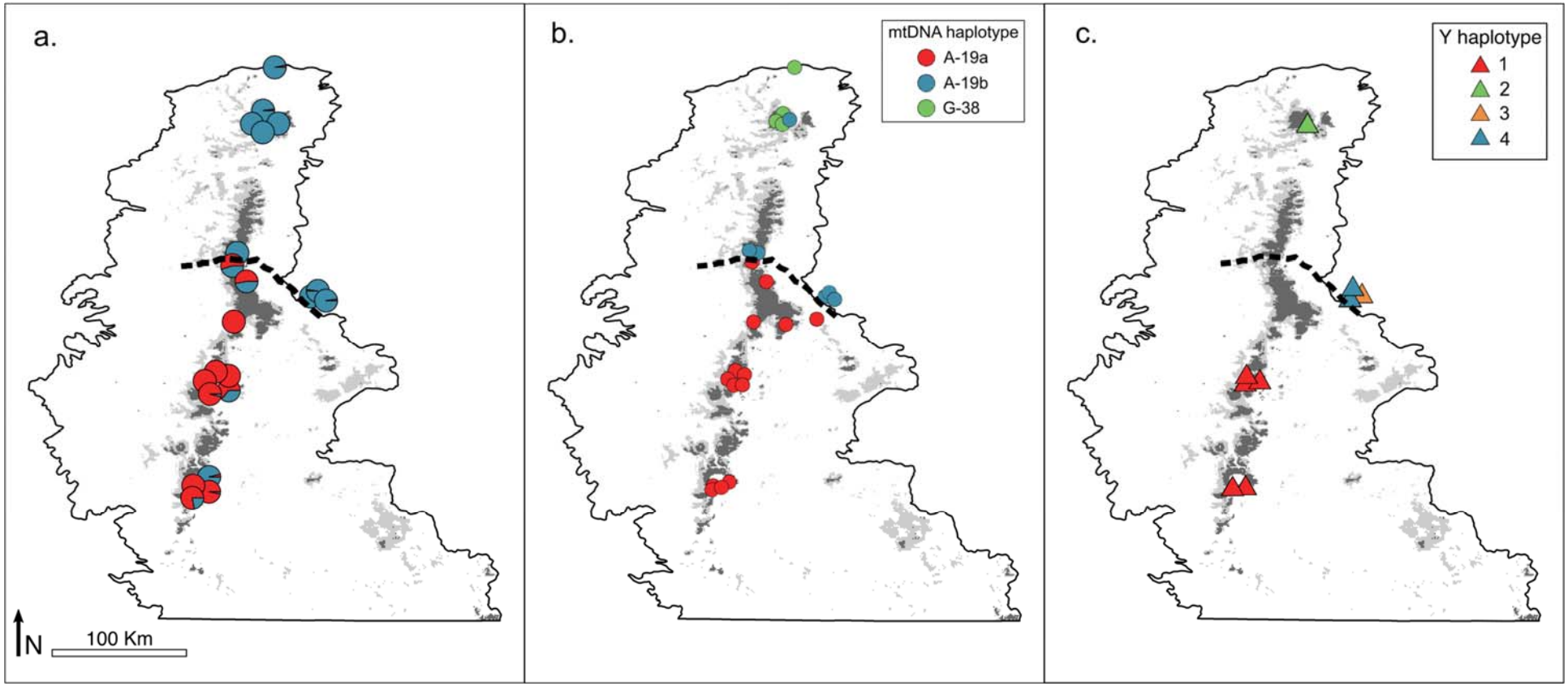

Figure 8. Map showing geographic break in genomic markers from red fox individuals sampled in the northern and southern portions of the Oregon Cascade ecoregion 2010-2016, with a contact zone mid-range corresponding approximately to Highway 20 (broken line). Symbols depict a single individual, showing a) proportion of individual ancestry (pie charts) estimated using 31 autosomal microsatellites in admixture program Structure at K = 2 genetic clusters (n = 21), b) mitochondrial haplotype (n = 19), and c) Y microsatellite haplotype (n = 9).

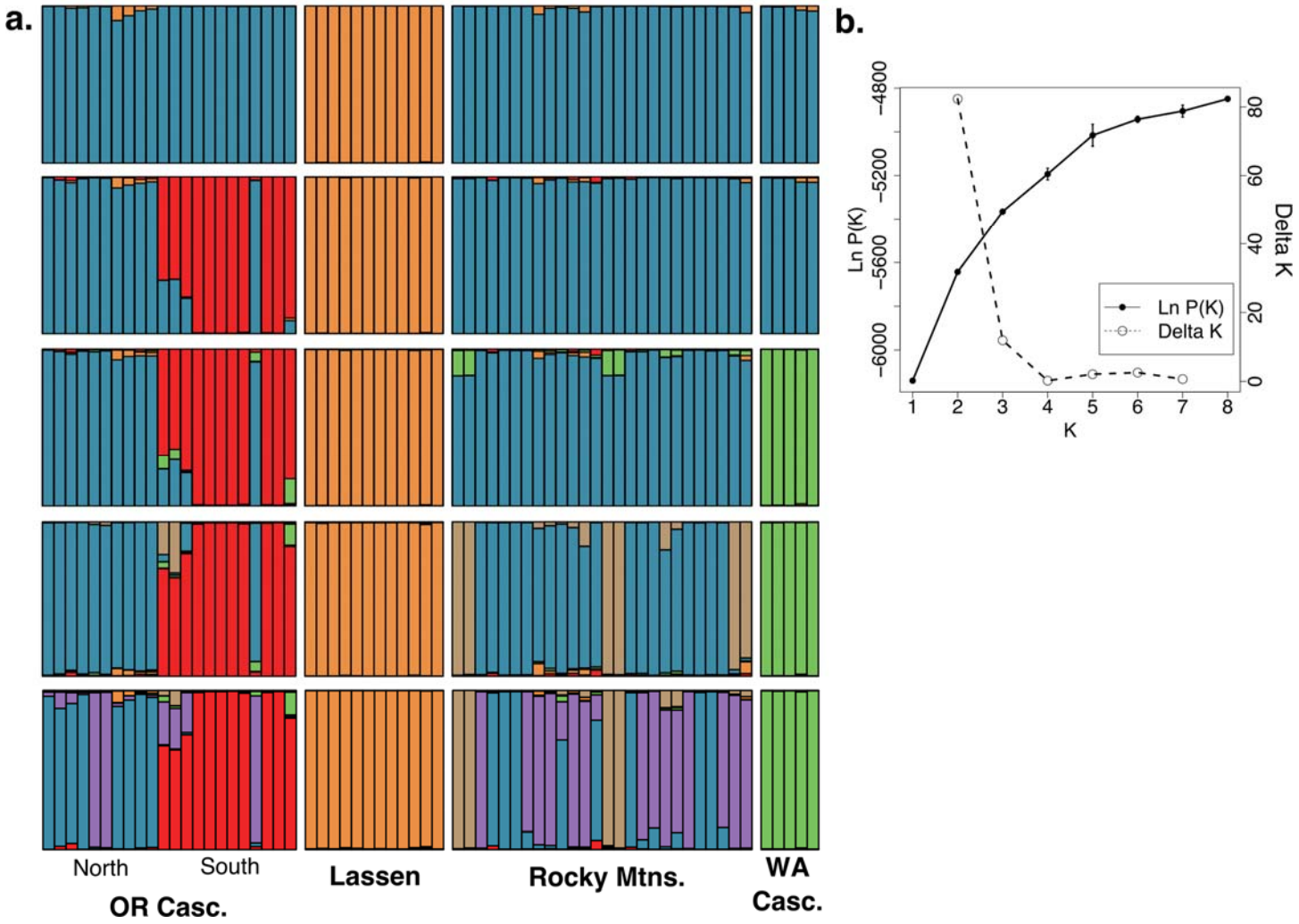

Figure 9. a) Structure results for the Oregon Cascade and other montane populations of red fox at K = 2–6 using 31 autosomal microsatellites, indicating the southern Oregon Cascade, Lassen, and the Washington Cascade consistently form distinct populations. b) Diagnostic plot for Structure admixture results, showing lack of agreement for the best number of K genetic clusters: K = 2 had highest support based on the mode of delta K values, and likelihood of the data continued to show small gains as K clusters increased from 4 to 8.

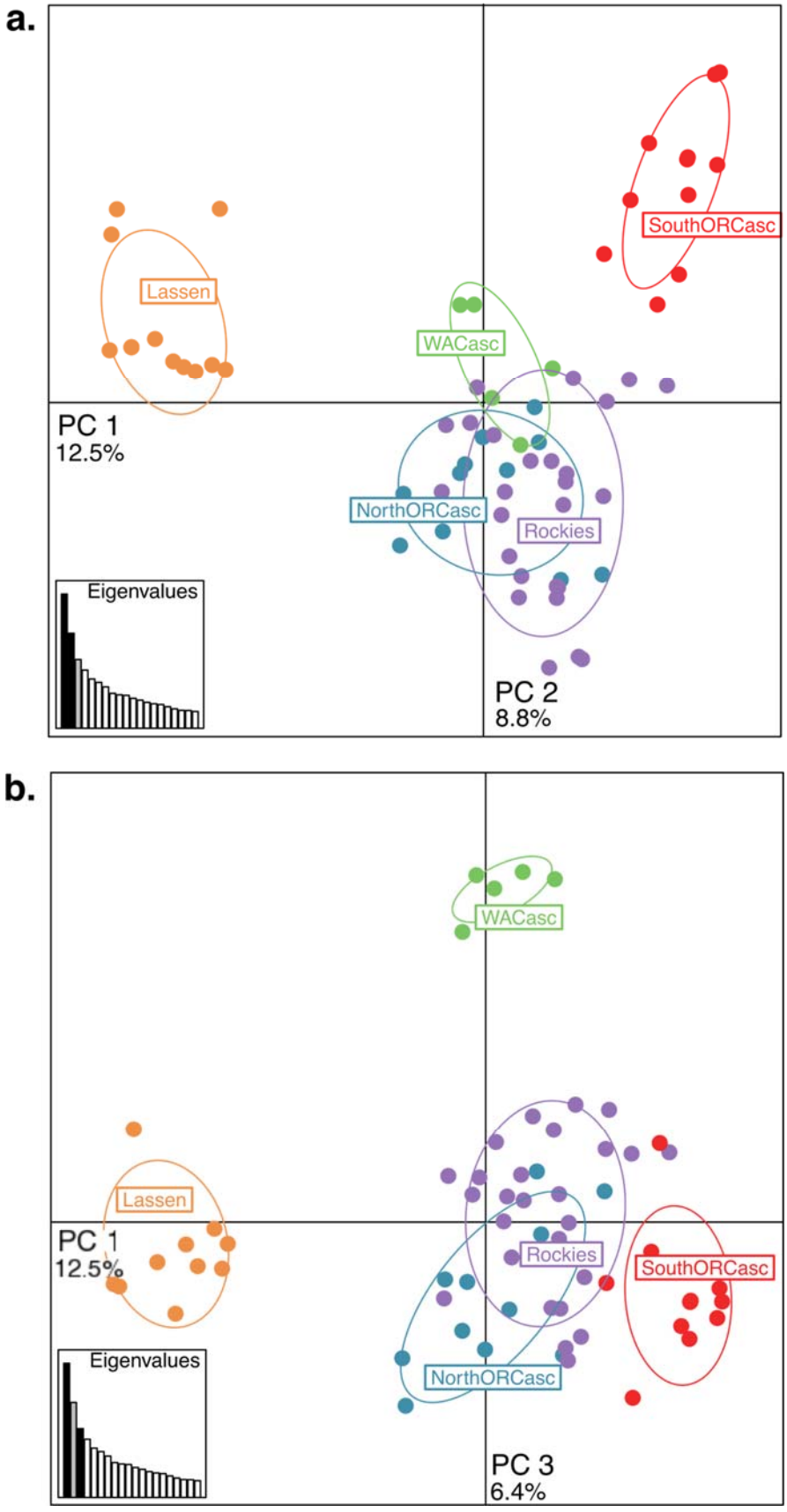

Figure 10. Principle component plots of montane red fox samples used in Structure analysis (Fig 9.), showing a) differentiation of the Lassen population and the southern Oregon Cascade population, and b) the Washington Cascade population along axis 3.

Appendix 1. Non-genetic occurrence records of red fox in the Oregon Cascade ecoregion (n = 97), including contemporary detections collected 2010–2016 (n = 76), and past records from 1985–1999 (n = 21). Detections were used in Maxent species distribution modeling (confirmed records n = 52; opportunistic sighting records dataset n = 45) after filtering to retain one record per 4 km^2.

Detection Type	Method	Administrative Unit	Source	Lat	Lon	Elev (m)	Date
Photograph	Carnivore Survey	Willamette National Forest	McFadden-Hiller and Hiller 2015	44.24822	-121.83495	1545	2013-2014
Photograph	Carnivore Survey	Deschutes National Forest	McFadden-Hiller and Hiller 2015	44.26927	-121.78003	1552	2013-2014
Photograph	Carnivore Survey	Deschutes National Forest	McFadden-Hiller and Hiller 2015	43.98984	-121.56020	1762	2013-2014
Photograph	Carnivore Survey	Deschutes National Forest	McFadden-Hiller and Hiller 2015	44.16728	-121.71237	1807	2013-2014
Photograph	Carnivore Survey	Deschutes National Forest	McFadden-Hiller and Hiller 2015	44.49142	-121.83164	1685	2013-2014
Photograph	Carnivore Survey	Deschutes National Forest	McFadden-Hiller and Hiller 2015	43.99384	-121.65555	1988	2013-2014
Photograph	Carnivore Survey	Deschutes National Forest	McFadden-Hiller and Hiller 2015	43.98165	-121.60668	1791	2013-2014
Photograph	Carnivore Survey	Willamette National Forest	McFadden-Hiller and Hiller 2015	44.46067	-121.85014	1816	2013-2014
Photograph	Carnivore Survey	Deschutes National Forest	McFadden-Hiller and Hiller 2015	44.15198	-121.63374	1667	2013-2014
Photograph	Carnivore Survey	Mount Hood National Forest	Cascadia Wild	45.40182	-121.73157	1707	10/5/2013
Photograph	Carnivore Survey	Crater Lake National Park	CRLA 2012 Red Fox Inventory	42.95719	-122.17444	2240	9/5/2013
Photograph	Carnivore Survey	Mount Hood National Forest	Cascadia Wild	45.33913	-121.73295	1783	5/16/2013
Photograph	Carnivore Survey	Mount Hood National Forest	Cascadia Wild	45.32735	-121.67114	1722	4/4/2013
Photograph	Carnivore Survey	Willamette National Forest	USFS NRIS Database	43.63916	-122.03943		3/18/2013
Photograph	Carnivore Survey	Mount Hood National Forest	Cascadia Wild	45.33969	-121.63381	1433	3/14/2013
Photograph	Carnivore Survey	Willamette National Forest	USFS NRIS Database	43.63923	-122.03958		3/8/2013
Photograph	Carnivore Survey	Rogue River - Siskiyou National Forest	USFS NRIS Database	43.09375	-122.28413		2/2/2013
Photograph	Carnivore Survey	Mount Hood National Forest	Cascadia Wild	45.39353	-121.65544	1920	1/13/2013
Photograph	Carnivore Survey	Mount Hood National Forest	Cascadia Wild	46.32922	-122.66773	1646	11/16/2012
Photograph	Carnivore Survey	Mount Hood National Forest	Cascadia Wild	45.39626	-121.64939	1798	9/9/2012
Photograph	Carnivore Survey	Crater Lake National Park	CRLA 2012 Red Fox Inventory	42.92914	-122.03955	2377	8/24/2012
Photograph	Carnivore Survey	Crater Lake National Park	CRLA 2012 Red Fox Inventory	42.89014	-122.07763	2275	8/20/2012
Photograph	Carnivore Survey	Crater Lake National Park	CRLA 2012 Red Fox Inventory	42.90665	-122.14860	2129	8/16/2012
Photograph	Carnivore Survey	Crater Lake National Park	CRLA 2012 Red Fox Inventory	42.95177	-122.18079	2241	8/12/2012
Photograph	Carnivore Survey	Crater Lake National Park	CRLA 2012 Red Fox Inventory	42.93703	-122.17411	2184	8/11/2012
Photograph	Carnivore Survey	Crater Lake National Park	CRLA 2012 Red Fox Inventory	42.89026	-122.08161	2314	8/8/2012
Photograph	Carnivore Survey	Crater Lake National Park	CRLA 2012 Red Fox Inventory	42.94602	-122.17866	2193	8/4/2012
Photograph	Carnivore Survey	Mount Hood National Forest	Cascadia Wild	45.33882	-121.73244	1768	4/23/2012
Photograph	Carnivore Survey	Mount Hood National Forest	Cascadia Wild	45.33654	-121.63031	1433	2/23/2012

Photograph	Carnivore Survey	Mount Hood National Forest	Cascadia Wild	45.39174	-121.65963	1981	1/10/2012
Photograph	Carnivore Survey	Crater Lake National Park	CRLA 2012 Red Fox Inventory	42.98479	-122.12304	2109	9/22/2011
Photograph	Opportunistic	Crater Lake National Park	CRLA Incidental Observation Database	42.92739	-122.05608	2253	9/2/2013
Photograph	Opportunistic	Crater Lake National Park	CRLA Incidental Observation Database	42.93024	-122.02862	2328	8/27/2013
Photograph	Opportunistic	Crater Lake National Park	CRLA Incidental Observation Database	42.93191	-122.03657	2371	8/26/2013
Photograph	Opportunistic	Crater Lake National Park	CRLA Incidental Observation Database	42.92422	-122.06058	2262	8/5/2013
Photograph	Opportunistic	Crater Lake National Park	CRLA Incidental Observation Database	42.90940	-122.14128	2161	7/25/2013
Photograph	Opportunistic	Crater Lake National Park	CRLA Incidental Observation Database	42.94635	-122.04432	2208	7/21/2013
Photograph	Opportunistic	Crater Lake National Park	CRLA Incidental Observation Database	42.93485	-122.04126	2367	7/18/2013
Photograph	Opportunistic	Deschutes National Forest	Linda Turner, USFS	43.98985	-121.56828		7/2/2013
Photograph	Opportunistic	Crater Lake National Park	CRLA Incidental Observation Database	42.91141	-122.14195	2107	7/1/2013
Photograph	Opportunistic	Crater Lake National Park	CRLA Incidental Observation Database	42.91099	-122.14319	2157	6/30/2013
Photograph	Opportunistic	Deschutes National Forest	Linda Turner, USFS	43.98229	-121.52346		6/29/2013
Photograph	Opportunistic	Crater Lake National Park	CRLA Incidental Observation Database	42.91049	-122.14195	2161	6/28/2013
Photograph	Opportunistic	Crater Lake National Park	CRLA Incidental Observation Database	42.91187	-122.14987	2155	6/26/2013
Photograph	Opportunistic	Crater Lake National Park	CRLA Incidental Observation Database	42.91466	-122.15976	2143	6/26/2013
Photograph	Opportunistic	Crater Lake National Park	CRLA Incidental Observation Database	42.90970	-122.13800	2138	6/20/2013
Photograph	Opportunistic	Crater Lake National Park	CRLA Incidental Observation Database	42.86516	-122.16631	1835	6/18/2013
Photograph	Opportunistic	Crater Lake National Park	CRLA Incidental Observation Database	42.90976	-122.13709	2140	6/15/2013
Photograph	Opportunistic	Crater Lake National Park	CRLA Incidental Observation Database	42.89396	-122.13622	1953	5/3/2013
Photograph	Opportunistic	Crater Lake National Park	CRLA Incidental Observation Database	42.89628	-122.13604	1964	4/16/2013
Photograph	Opportunistic	Crater Lake National Park	CRLA Incidental Observation Database	42.89146	-122.13506	1948	12/6/2012
Photograph	Opportunistic	Crater Lake National Park	CRLA Incidental Observation Database	42.90140	-122.14696	2314	5/16/2012
Sighting	Opportunistic	Crater Lake National Park	CRLA Incidental Observation Database	42.92910	-122.02996	2344	9/11/2013
Sighting	Opportunistic	Crater Lake National Park	CRLA Incidental Observation Database	42.93281	-122.04044	2369	9/6/2013
Sighting	Opportunistic	Crater Lake National Park	CRLA Incidental Observation Database	42.98060	-122.15266	2112	9/1/2013
Sighting	Opportunistic	Crater Lake National Park	CRLA Incidental Observation Database	42.86992	-122.14420	1873	7/27/2013
Sighting	Opportunistic	Crater Lake National Park	CRLA Incidental Observation Database	42.92344	-122.06033	2266	7/27/2013
Sighting	Opportunistic	Crater Lake National Park	CRLA Incidental Observation Database	42.90959	-122.13914	2144	7/21/2013
Sighting	Opportunistic	Crater Lake National Park	CRLA Incidental Observation Database	42.91313	-122.07189	2047	7/21/2013
Sighting	Opportunistic	Crater Lake National Park	CRLA Incidental Observation Database	42.95096	-122.17367	2327	7/15/2013
Sighting	Opportunistic	Crater Lake National Park	CRLA Incidental Observation Database	42.86703	-122.16244	1832	7/7/2013
Sighting	Opportunistic	Crater Lake National Park	CRLA Incidental Observation Database	42.90287	-122.14239	2121	6/26/2013
Sighting	Opportunistic	Crater Lake National Park	CRLA Incidental Observation Database	42.90779	-122.12953	2278	6/25/2013

Sighting	Opportunistic	Crater Lake National Park	CRLA Incidental Observation Database	42.94325	-122.04124	2238	6/20/2013
Sighting	Opportunistic	Crater Lake National Park	CRLA Incidental Observation Database	42.90978	-122.13621	2154	6/15/2013
Sighting	Opportunistic	Crater Lake National Park	CRLA Incidental Observation Database	42.86219	-122.15801	1806	6/11/2013
Sighting	Opportunistic	Crater Lake National Park	CRLA Incidental Observation Database	42.88212	-122.09782	1980	6/11/2013
Sighting	Opportunistic	Crater Lake National Park	CRLA Incidental Observation Database	42.89523	-122.13719	2109	4/19/2013
Sighting	Opportunistic	Willamette National Forest	USFS NRIS Database	44.39600	-121.88402		4/12/2013
Sighting	Opportunistic	Willamette National Forest	USFS NRIS Database	43.62261	-122.04609		10/11/2012
Sighting	Opportunistic	Crater Lake National Park	CRLA Incidental Observation Database	42.86692	-122.14659	1846	7/2/2012
Sighting	Opportunistic	Willamette National Forest	USFS NRIS Database	43.83927	-122.27659		7/15/2011
Sighting	Opportunistic	Willamette National Forest	USFS NRIS Database	43.61240	-122.03595		12/1/2010
Sighting	Opportunistic	Willamette National Forest	USFS NRIS Database	43.60370	-122.03782		12/1/2010
Sighting	Opportunistic	Willamette National Forest	USFS NRIS Database	43.72017	-122.00632		10/1/2010
Track	Opportunistic	Willamette National Forest	USFS NRIS Database	44.44792	-121.84323		1/4/2013
Sighting	Opportunistic	Deschutes National Forest	USFS NRIS Database	44.46058	-121.64546		8/20/1999
Sighting	Opportunistic	Deschutes National Forest	USFS NRIS Database	43.35647	-121.76620	1390	6/26/1997
Sighting	Opportunistic	Rogue River - Siskiyou National Forest	USFS NRIS Database	42.76240	-122.48822	808	3/1/1993
Sighting	Opportunistic	Fremont-Winema National Forest	USFS NRIS Database	42.53819	-122.23122	1841	6/5/1992
Sighting	Opportunistic	Fremont-Winema National Forest	USFS NRIS Database	43.10075	-121.33915	1537	5/28/1992
Sighting	Opportunistic	Fremont-Winema National Forest	USFS NRIS Database	42.25357	-122.13766	1459	9/26/1991
Sighting	Opportunistic	Fremont-Winema National Forest	USFS NRIS Database	43.26783	-121.51317	1608	9/24/1991
Sighting	Opportunistic	Fremont-Winema National Forest	USFS NRIS Database	42.52083	-122.21884	1793	6/25/1991
Sighting	Opportunistic	Fremont-Winema National Forest	USFS NRIS Database	42.46664	-122.17866	1496	8/30/1990
Sighting	Opportunistic	Fremont-Winema National Forest	USFS NRIS Database	43.30381	-121.49393	1859	6/20/1990
Sighting	Opportunistic	Fremont-Winema National Forest	USFS NRIS Database	43.24966	-121.48135	1557	9/27/1989
Sighting	Opportunistic	Fremont-Winema National Forest	USFS NRIS Database	42.78818	-122.12202	1737	8/30/1989
Sighting	Opportunistic	Fremont-Winema National Forest	USFS NRIS Database	42.25357	-122.13766	1459	5/10/1989
Sighting	Opportunistic	Fremont-Winema National Forest	USFS NRIS Database	42.43611	-122.12762	1277	9/12/1988
Sighting	Opportunistic	Fremont-Winema National Forest	USFS NRIS Database	42.23575	-122.06097	1328	9/22/1986
Sighting	Opportunistic	Deschutes National Forest	USFS NRIS Database	43.55275	-121.78581	1592	6/28/1986
Sighting	Opportunistic	Deschutes National Forest	USFS NRIS Database	43.54209	-121.90136	1569	6/10/1986
Sighting	Opportunistic	Deschutes National Forest	USFS NRIS Database	43.29017	-121.75564	1457	6/3/1986
Sighting	Opportunistic	Deschutes National Forest	USFS NRIS Database	43.29265	-121.74409	1592	1/1/1986
Sighting	Opportunistic	Deschutes National Forest	USFS NRIS Database	43.55529	-121.82473	1890	10/9/1985

Sighting	Opportunistic	Fremont-Winema National Forest	USFS NRIS Database	43.27647	-121.73844	1517	6/4/1985

Appendix 2. Environmental layers considered for Maxent modeling of red fox distribution in the Oregon Cascade ecoregion, prior to using variance inflation factor (VIF) to exclude variables with pairwise correlations >0.7.

Category	Code	Environmental Layer	Source
Climate	Tmean	Mean annual temperature	PRISM 30-year normal (800 m)
Climate	Tmax	Maximum annual temperature	PRISM 30-year normal (800 m)
Climate	Tmin	Minimum annual temperature	PRISM 30-year normal (800 m)
Climate	PPT	Annual precipitation	PRISM 30-year normal (800 m)
Climate	$Tmin_{Dec}$	Minimum December temperature	PRISM 30-year normal (800 m)
Climate	$TMin_{Jan}$	Minimum January temperature	PRISM 30-year normal (800 m)
Climate	$Tmin_{Feb}$	Minimum February temperature	PRISM 30-year normal (800 m)
Climate	$Tmax_{June}$	Maximum June temperature	PRISM 30-year normal (800 m)
Climate	$Tmax_{July}$	Maximum July temperature	PRISM 30-year normal (800 m)
Climate	$Tmax_{Aug}$	Maximum August temperature	PRISM 30-year normal (800 m)
Climate	BIO2	Mean Diurnal Range (Mean of monthly)	Worldclim BIO2
Climate	BIO3	Isothermality (BIO2/BIO7) (* 100)	Worldclim BIO3
Climate	BIO4	Temperature Seasonality (standard deviation *100)	Worldclim BIO4
Climate	BIO7	Temperature Annual Range (BIO5-BIO6)	Worldclim BIO7
Climate	BIO8	Mean Temperature of Wettest Quarter	Worldclim BIO8
Climate	BIO9	Mean Temperature of Driest Quarter	Worldclim BIO9
Climate	BIO10	Mean Temperature of Warmest Quarter	Worldclim BIO10
Climate	BIO11	Mean Temperature of Coldest Quarter	Worldclim BIO11
Climate	BIO13	Precipitation of Wettest Month	Worldclim BIO13
Climate	BIO14	Precipitation of Driest Month	Worldclim BIO14
Climate	BIO15	Precipitation Seasonality (Coefficient of Variation)	Worldclim BIO15
Climate	BIO16	Precipitation of Wettest Quarter	Worldclim BIO16
Climate	BIO17	Precipitation of Driest Quarter	Worldclim BIO17
Climate	BIO18	Precipitation of Warmest Quarter	Worldclim BIO18
Topography	Slope	Slope	USGS DEM (1 arc-second)
Topography	Aspect	Transformed aspect (incident radiation)	USGS DEM (1 arc-second)
Topography	Rough	Roughness	USGS DEM (1 arc-second)
Vegetation	Gap	GAP land-cover category	NW ReGAP 2010
Vegetation	Cancov	Percent canopy cover	LEMMA GNN

Appendix 3. Classification of land-cover types in ReGAP layer for Maxent distribution model of red fox in the Oregon Cascade ecoregion.

ReGAP Name	ReGAP Code	Maxent Class	Maxent Code	% Back-ground	Red Fox Detected?
Water	43	Water	1	0.019	-
Old Field, Abandoned Cropland, Clearcuts, CRP	31	Disturbed	2	0.105	Y
Developed Open Space	45	Disturbed	2	-	-
Rural Residential	34	Disturbed	2	-	-
Suburban	41	Disturbed	2	-	-
Urban	42	Disturbed	2	-	-
Urban	42	Disturbed	2	-	-
High Structure Agriculture	19	Disturbed	2	-	-
Pasture/Hay	32	Disturbed	2	-	-
Cultivated Crops	14	Disturbed	2	-	-
High Structure Agriculture	19	Disturbed	2	-	-
Alpine and Subalpine Habitats	3	Alpine	4	0.01	Y
Lava Flows	23	Lava	6	0.015	Y
Marshes, Bogs and Emergent Wetlands	25	Wetlands	10	0.016	-
Mixed Conifer Forests	26	Mixed Conifer	13	0.379	Y
Siskiyou Mixed Conifer Forests and Woodlands	39	Mixed Conifer	13	-	-
Juniper Woodlands and Savanna	21	Juniper Woodlands and Savanna	16	0.006	-
Mixed Hardwood-Conifer Forests	27	Mixed Hardwood-Conifer Forests	17	0.014	-
Subalpine Forests and Woodlands	40	Subalpine Forest	18	0.042	Y
Chaparral	7	Chaparral	19	0.003	-
Silver Fir - Mountain Hemlock Montane Forests	38	Silver Fir - Mt Hemlock	20	0.169	Y
Lodgepole Pine Forests and Woodlands	24	Lodgepole	21	0.065	Y
Ponderosa Pine Forests and Woodlands	33	Ponderosa	22	0.145	Y
Low, Rigid, Black and Early Sagebrush Shrublands and Steppe	8	Sagebrush	24	0.004	-
Columbia Basin Grasslands and Prairie	13	Columbia Basin Grassland	27	0.001	-
Montane Grasslands and Meadows	28	Montane Meadow	28	0.003	Y
Forest/Shrub Swamps	18	Forest/Shrub Swamp	32	0.001	-

Appendix 4. Selection indices for 9 uncorrelated environmental layers estimated using red fox occurrence and background points within a 20-km radius, prior to Maxent distriubiton modeling in the Oregon Cascades. Selection was caluclated from using ln(observed occurrences/expected occurrences + 1) – ln(2). Positive and negative numbers indicate use of an environmental category proportionately greater and less than expected based on the composition of the study area.

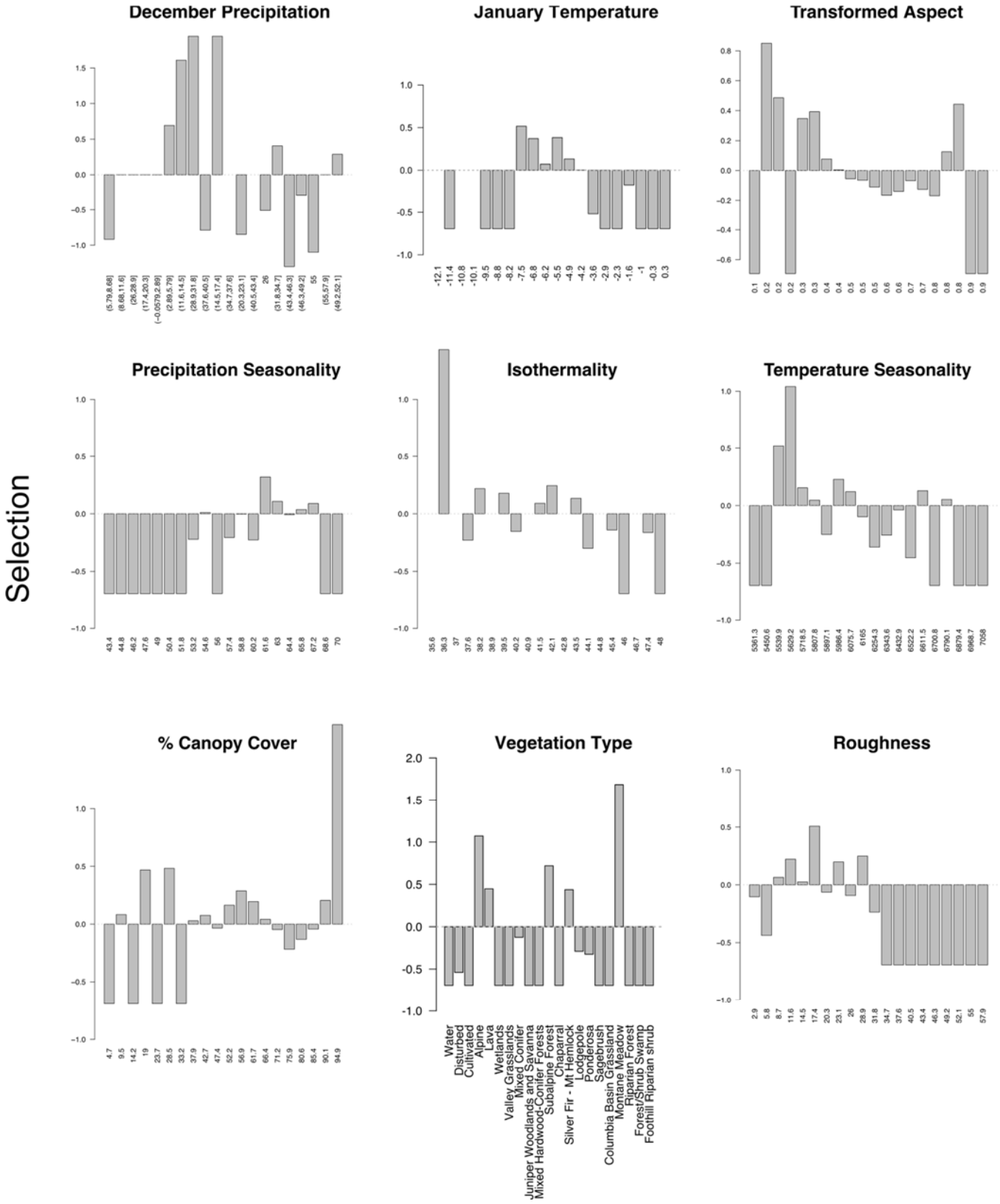

Appendix 5. The Maxent modeled response of probability of red fox occurrence in the Oregon Cascades based on 9 uncorrelated environmental variables. Response curves are shown from the confirmed and inclusive datasets at default (a, c) and optimal (b, d) regularization settings, illustrating the tendency of higher regularization to dampen the response of modeled weak relationships.

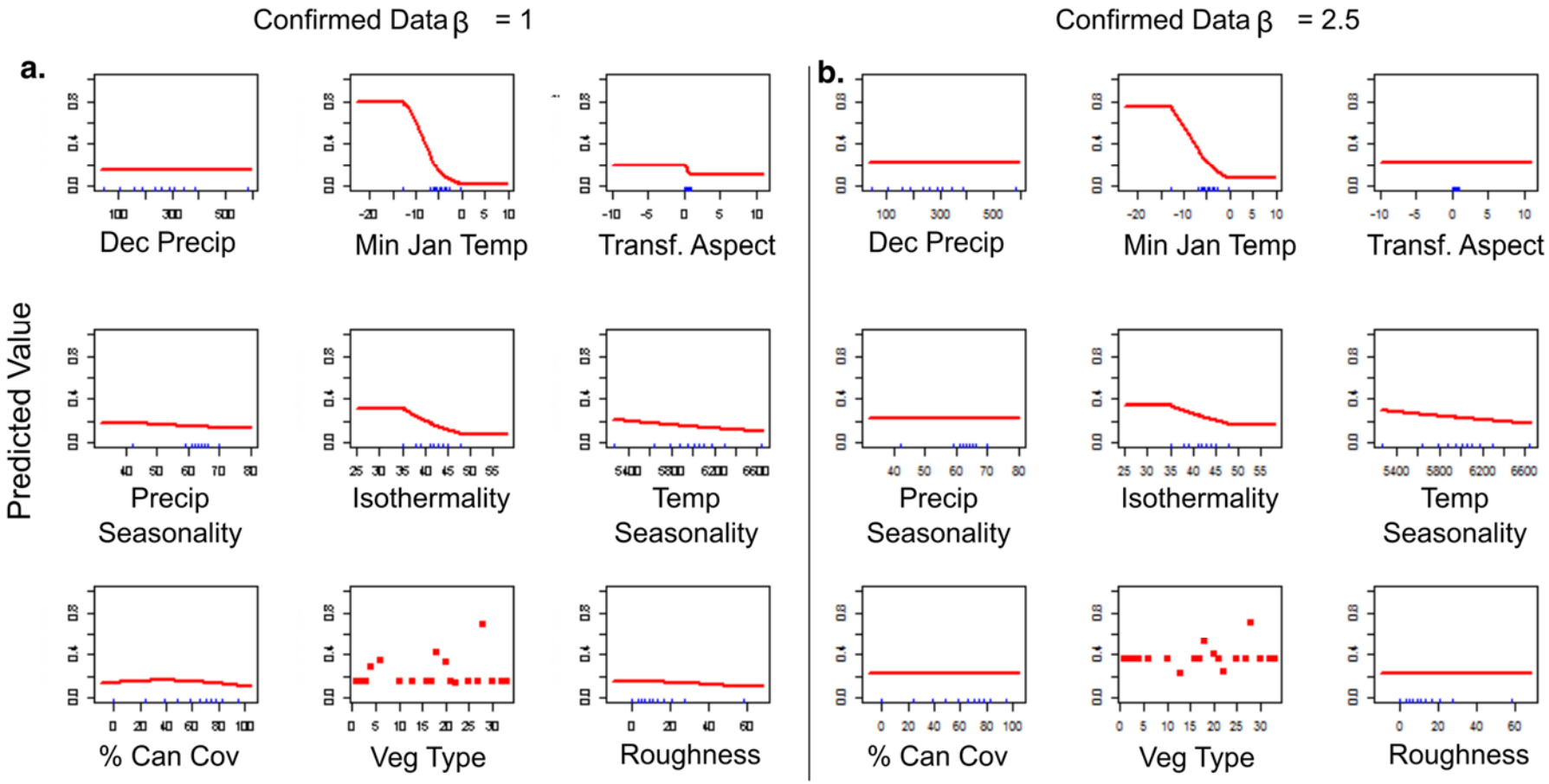

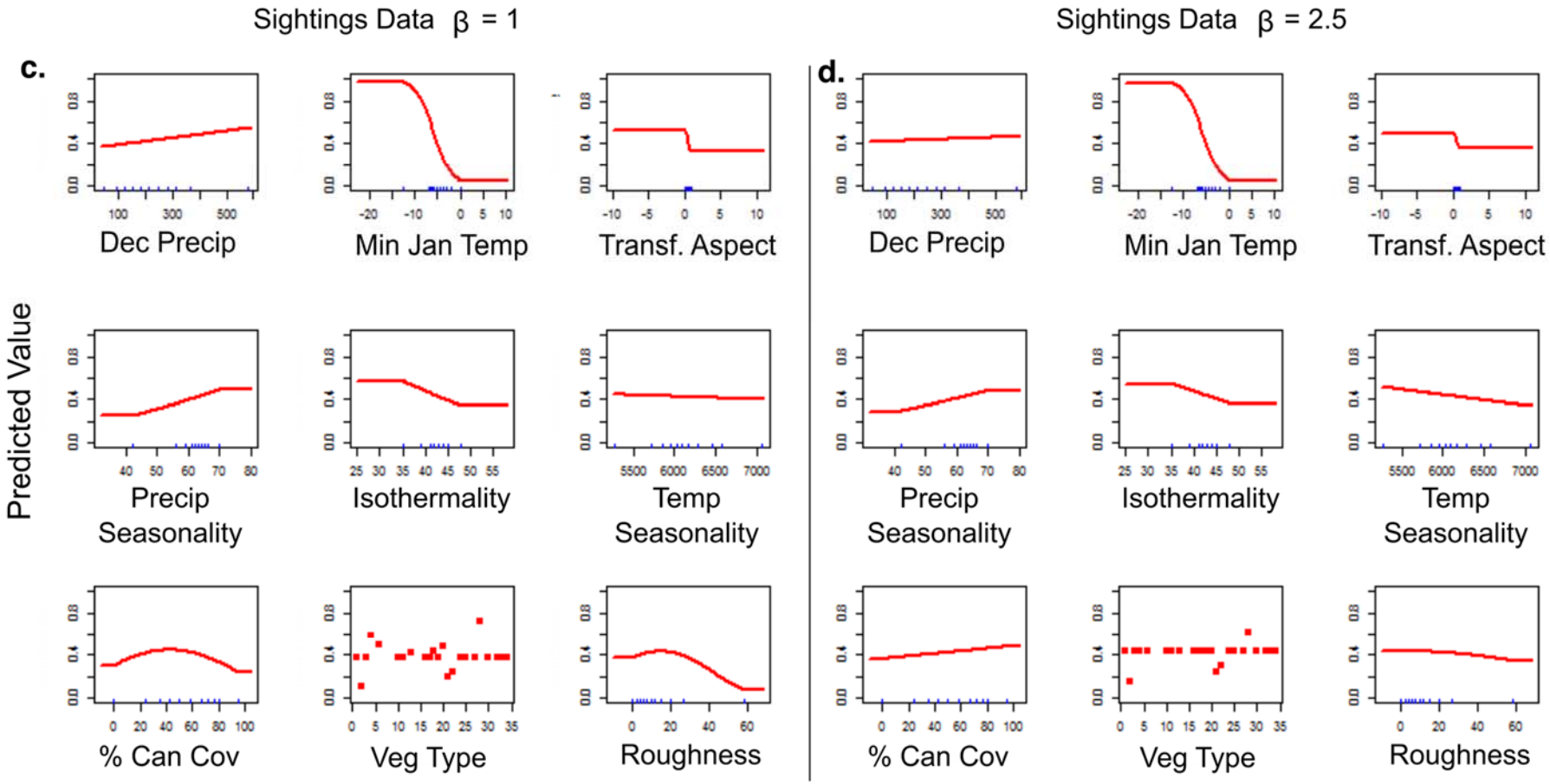
Sightings Data β = 1
Sightings Data β = 2.5
c.
d.
Predicted Value
Dec Precip
Min Jan Temp
Transf. Aspect
Precip Seasonality
Isothermality
Temp Seasonality
% Can Cov
Veg Type
Roughness

Appendix 6. a) Proportion of occurrence and background points included in predicted presence surface according to the probability value selected as a threshold. Optimal threshold probability values (black fill circles) were chosen to promote discriminatory power, as determined by b) maximizing the difference in the proportions of occurrence and background points included in the predicted presence surface. In principle optimal thresholds should balance the amount of area predicted as presence (specificity) and the proportion of known occurrence records omitted from predicted area (1- sensitivity).